Remote Sensing Of Environment
April 2019, Volume 224 Pages 275-288
https://doi.org/10.1016/j.rse.2019.01.028
https://archimer.ifremer.fr/doc/00482/59395/

Archimer
https://archimer.ifremer.fr

Toward science-oriented validations of coastal altimetry: Application to the Ligurian Sea

Meloni M. [1,*], Bouffard J. [2], Doglioli A.M. [3], Petrenko A.A. [3], Valladeau G. [4]

[1] Serco, Via Sciadonna n.24, Frascati, Italy
[2] ESA (European Space Agency), Earth Observation Directorate, Via Galileo Galilei, 2–00044 Frascati, Italy
[3] Aix Marseille Univ., Université de Toulon, CNRS, IRD, MIO UM 110, 13288, Marseille, France
[4] CLS (Collecte Localisation Satellites), 11 Rue Hermes, 31520 Ramonville-Saint-Agne, France

* Corresponding author : M. Meloni, email address : marco.meloni@serco.com

Abstract :

This study is a preliminary contribution to the European Space Agency's efforts aimed at establishing reference in situ networks specifically targeted to validate coastal altimetry. For this purpose, we processed and cross-compared conjointly improved altimetry data and in situ measurements acquired over the Ligurian Sea – a coastal region of the Mediterranean characterised by complex, fine-scale and rapidly evolving oceanic features. We made use of several kinds of multi-sensor in situ observations located along SARAL and Jason-2 tracks. The main objectives of the study were to assess improved coastal oriented validation strategies, including the usage of a new in situ platform (Moving Vessel Profiler), while better understanding potential differences owing to physical content inconsistency and instrumental or data processing limitations. The results show remarkable agreements over spatial scales of few tens of kilometres, paving the way for the deployment of future in situ networks and the definition of science-oriented diagnostics targeted to assess the capability of present and future high-resolution altimetric missions in resolving small-scale physical features.

Highlights

► Validating coastal altimetry in fine-scale dynamics areas is challenging. ► *Ad-hoc* multi-platform validation approaches required. ► Measurements from the MVP are very promising for validating coastal altimetry. ► The combined use of collocated MVP, altimetry and ADCP appear to be relevant.

Keywords : Coastal altimetry, Mesoscale, Validation and verification, Northern current

Please note that this is an author-produced PDF of an article accepted for publication following peer review. The definitive publisher-authenticated version is available on the publisher Web site.

1 Introduction

Even if coastal zones cover only 8% of the entire ocean surface of the earth (Stanev et al., 2002), they play a crucial role for global ocean circulation, as it provides dynamical boundary layers for physical, chemical and biological processes. Coastal regions are characterised by complex ocean dynamics; they are often dominated by small and rapidly evolving mesoscale/sub-mesoscale structures (hereafter "(sub-)mesoscale"), which play a major role in the transport of heat, salt and biogeochemical tracers (McGillicuddy et al., 1998; Levy and Martin, 2013; Mahadevan, 2016) and significantly influence water-mass mixing and exchanges between the continental shelf and the open ocean (Huthnance, 1995; Muller-Karger et al., 2005). Despite their importance, the high spatial/temporal variability and complexity associated with (sub-)mesoscale dynamics make them difficult to study with sparse *in situ* observations (Nencioli et al., 2013), requiring the development of modelling at kilometric (Thomas et al., 2008) and sub-kilometric horizontal space grids (Gula et al., 2014; Shcherbina et al., 2013) as well as the use of high-resolution satellite observations (Lehahn et al., 2007; Fu and Ferrarri, 2008; Bouffard et al., 2014; Hu et al., 2011). The issue of characterising (sub-)mesoscale processes is particularly critical over the coastal domain, where the local Rossby radius is smaller than in the open-ocean (Hallberg, 2013).

Over the last three decades, progress in satellite altimetry has contributed to revolutionising physical oceanography, enabling the global characterization of open-ocean large scale and mesoscale processes (Pascual et al., 2010, 2013; Fu et al., 2001). Satellite altimeters are particularly well adapted for observing open-ocean structures (Fu et al., 2010) and represent an invaluable source of data, providing repetitive views of phenomena unachievable by other means (Fu and Chelton, 2001). One of the main challenges for the next decade is the characterisation of fine-scale processes in the coastal domain (Cipollini et al., 2009). Achieving this goal requires not only the innovation of space-born instruments and processing techniques but also establishing *ad-hoc* validation approaches, allowing better assessment of potential improvements regarding the precision and accuracy of retrieved geophysical parameters. Increasingly more multi-disciplinary *in situ* data acquired by marine observatories and oceanographic campaigns are now being made available (Palacz et al., 2017) and can be used to derive quality indicators for coastal altimetry based on the assessment of along-track sea surface gradients complementary to the assessment of sea surface time series from tide gauges (Bonnefond et al., 2018). Here, we propose exploiting such *in situ* data resources to quantify the potential benefit of innovative coastal altimetry processing techniques for the characterization of small-scale ocean geostrophic currents.

Several previous studies have evaluated the capabilities of conventional pulse-limited Ku-Band altimetry to observe mesoscale dynamics in semi-enclosed seas, such as the Mediterranean Sea (Vignudelli et al., 2005; Bouffard et al., 2008a, 2008b, 2011; Birol and Delebecque, 2014; Birol and Niño, 2015; Jebri et al., 2017). Despite significant advances, new coastal-oriented processing techniques require continuous optimisation and refinement by being systematically cross-compared with collocated multi-platform measurements. Over the last decade, several cruise campaigns using ship and glider measurements along with altimeter tracks have been carried out in the Western Mediterranean Sea (Ruiz et al., 2012). For example, in Ruiz et al.'s (2009) study, glider- and ship-based measurements were performed under an ENVISAT track in order to provide a mesoscale description of the Balearic Front. Coastal and mesoscale dynamics analysis using conventional altimetry and gliders have also been described by Bouffard et al. (2010, 2012) and Aulicino et al. (2018) over the Balearic Sea and the Algerian Basin respectively. More recently, significant improvements have been obtained as a result of the advent of new technologies, such as Ka-band measurements from SARAL (Verron et al., 2015; Troupin et al. 2015; Pascual et al., 2015) and SAR altimetry measurements from the CryoSat-2 and Sentinel-3 missions (Bonnefond et al., 2018; Pascual et al., 2017; Morrow et al., 2017; Dinardo et al., 2017; Heslop et al., 2017; Bouffard et al., 2017; Calafat et al., 2016).

The goal of the present paper is to go one step further in the fine cross-analysis of coastal altimetry data and *in situ* measurements by determining the potential source of disagreements due to measurement errors and data processing limitations with respect to expected differences arising from physical content inhomogeneity and *in situ* reference level issues. Here, we utilise both Moving Vessel Profiler (MVP) and Acoustic Doppler Current Profiler (ADCP) acquired during the OSCAHR (Observing Submesoscale Coupling at High Resolution, Doglioli, 2015) Campaign along SARAL and Jason-2 altimetric tracks. We focus our analysis on the impact assessment of coastal-oriented altimetry processing strategies specifically developed and tested with experimental high frequency PEACHI products (Valladeau et al., 2015). The obtained improvements are discussed with respect to regional 1Hz AVISO Sea Level Anomaly products (http://aviso.altimetry.fr/). Two kinds of Mean

Dynamic Topographies (MTDs) have been also used and analysed in order to reconstruct Absolute Dynamic Topography (ADT).

After describing the study area and the characteristics of the *in situ* and space-based datasets used, the derived absolute geostrophic currents are compared to both ADCP and MVP measurements, which, in our knowledge, are used conjointly for the first time to evaluate coastal altimetry strategies. The paper then focuses on the quantitative and qualitative analysis of depicted ocean features, providing a critical discussion on the limitations and uncertainty associated with each observing system.

2 Study Areas

Although the issues addressed in this paper are of global relevance, its primary focus is on the North-Western Mediterranean (NWMed) Sea with particular emphasis on the Ligurian Sea area. Figure 1 shows the bathymetry of the selected area along with altimetry tracks (black lines), *in situ* measurements and the general circulation patterns.

The regional dynamics of the area is dominated by a cyclonic gyre circulation, the northern part of which is known as the “Liguro-Provençal Current” (Millot, 1991, 1999) or the “Northern Current” (NC) (Millot and Taupier Letage, 2005). This slope current arises from the merging of the eastern and western Corsica currents in the Ligurian Basin. It then flows to the southwest along the continental slope until it reaches the Balearic Sea. The NC exhibits a permanent surface density front between the lighter coastal waters and the denser waters found offshore, generating a sea surface high gradient in the across-shore direction.

Several numerical studies (Barrier et al., 2016; Zakardjan and Prieur, 1998) and observations along the path of the NC, such as hydrographic measurements from R/V cruises and HF radar (Forget et al., 2006; Marmain et al., 2014) describe this current as a complex dynamical feature marked by a large spectrum of spatial and temporal scales of variability. The NC is relatively narrow (~30–75 km) and its mean position lies within 60 km off the coast (Petrenko, 2003). The core of the NC is stronger and located about 10–40 km away from the coast in winter, while it is less defined and further offshore in late summer and early fall (Birol et al., 2010; Piterbarg et al., 2014; Declerck et al., 2016).

Glider transects across the NC have been performed in the Ligurian Sea, such as in Cyr et al. (2017) and during the MOOSE project (Quentin et al., 2013). Two different parts constitute the main cyclonic circulation over this area: a small recirculation centred on the grey arrow in Figure 1 and a second one in the southwest separated by a local minimum in current intensity (Marrec et al., 2018). The ADT signature associated with this fine-scale circulation can be potentially observed using satellite altimetry measurements (Bouffard, 2010). However, monitoring coastal dynamics from space is still challenging because of the numerous instrumental and geophysical limitations in addition to the fact that the altimeter footprints may encounter the coastline, corrupting the raw along-track remote-sensed signal (Anzenhofer et al., 1999; Strub, 2001).

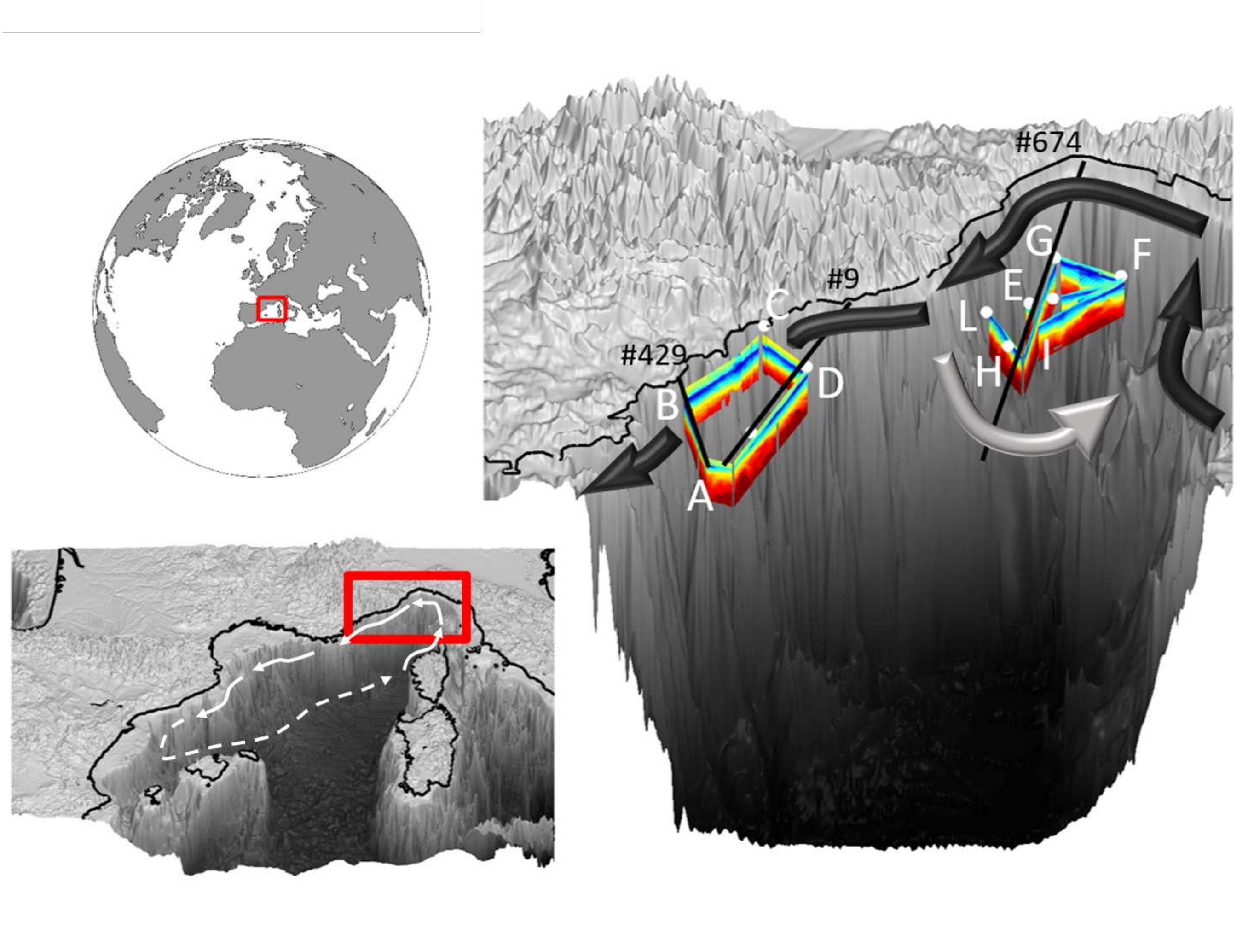

Figure 1 OSCAHR cruise transects (in letters) showing MVP vertical salinity profiles (coloured rectangles), geo-located with altimetric tracks #9 from Jason-2 and tracks #429 and #674 from SARAL. The main flow of the NC is shown with black arrows, the recirculation with a grey arrow and the Ligurian Sea area is highlighted by the red box.

3 Data and Methods

3.1 *In situ* observations

The *in situ* observations used in our study were acquired during the OSCAHR campaign (Doglioli, 2015), whose scientific objectives included the characterisation of a sub-mesoscale dynamical structure and study of its influence on the distribution of biogenic elements and the structure and dynamics of the first trophic levels (Marrec et al., 2018). The cruise strategy utilises an adaptive approach based on the near real-time analysis of both satellite data and numerical modelling in order to identify the dynamical features of interest and track their evolution. Apart from its main scientific objectives regarding (sub-)mesoscale physical/biochemistry coupling the OSCAHR campaign also aims to validate new remote-sensing retrieval techniques (altimetry, ocean colour, planktonic assemblage reconstruction) and high-resolution numerical modelling. In particular, we performed *in situ* measurements along three altimetric tracks shown in Figure 1 in the present study. The satellite and vessel passages are summarised in Table 1.

The R/V Téthys II is equipped with a hull-mounted ADCP RDI Ocean Sentinel 75 kHz; however, the methodology considered in this paper includes the usage of novel platforms of observation for sampling the ocean sub-surface layer at a high spatial and temporal frequency. In particular, we use a MVP200 equipped with a MSFFF I (Multi-Sensor Free Fall Fish type I). A total of 448 casts were performed along a 366-km route (55 hours of effective work). During the free fall, for each cast, measurements of temperature, salinity and pressure were performed with a temporal resolution of 8–10 min, corresponding to a spatial horizontal resolution of ~ 1 km. The CTD (Conductivity Temperature and Depth) sensor mounted in the MVP towed fish has the following precisions: ±0.005 [°C] for temperature and ±0.01 [mS cm-1] for conductivity. The density is estimated using the TEOS-10 (Thermodynamic Equation of Seawater) equation of state of seawater. Thereafter, temperature, salinity and density fields were used to estimate the Dynamic Height (DH) with respect to an arbitrary, no-motion reference level. This reference level is generally chosen to be at the maximum depth reached by the probe. Following Pond et al., (1986):

$$\mathrm{DH} = \int \delta(\mathrm{T}, \mathrm{S}, \mathrm{p})\mathrm{dp} \qquad (1)$$

where:

$$\delta(T,S,p) = \rho(T,S,p)^{-1} - \rho(0,35,p)^{-1} \quad (2)$$

δ is the specific volume anomaly, i.e., the difference in volume between a unit mass of water at temperature T, salinity S and pressure p and a unit mass at the temperature T = 0°C, salinity S = 35.0 and pressure p.

In a local Cartesian coordinate with *x* axis pointing East, *y* axis pointing North, the geostrophic approximation is then applied to compute the MVP-derived current:

$$V = \frac{f}{g} \cdot \frac{dh}{dx} \quad (3)$$

where f is the Coriolis parameter, g is gravity (9.8 m s^{-2}) and h is the DH.

MVP-derived relative DH and geostrophic current (with respect to reference depth) were compared with the geo-located SARAL and Jason-2 altimetry-derived absolute ADT and currents (with respect to the geoid). As compared to ocean gliders, using MVP has three main advantages: i) the probe performs free fall vertical profiles; ii) the sampling rate is higher and iii) the planned route (e.g., the altimetric track) is better followed, being the exact probe wed by the vessel. On the other hand, the main limit is a lower maximum operating depth. Subsequently, to understand the impacts of the reference depth and ageostrophic motions in the altimetry versus MVP comparisons, ADCP measurements were also considered in this study. The ADCP configuration used during the whole cruise included 60 cells, 8 m depth bins, an ensemble average of 1' and bottom tracking when possible (although most of the cruise took place out of reach of the bottom). The depth range extends from 18.5 m to 562.5 m with a vertically averaged error of 3.6 cm/s.

Table 1 Satellite *in situ* (MVP + ADCP) synchronization

Trace	Satellite Passage	Beginning waypoint	MVP Start	Ending Waypoint	MVP end	Time Diff.
Jason-2 #9	31/10/15 16:56	D	30/10/15 15:30	A	30/10/15 23:30	-21 h
SARAL #429	30/10/15 05:02	A	31/10/15 01:30	B	01/11/15 06:30	+35 h
SARAL #674	07/11/15 18:02	G	03/11/15 23:00	I	04/11/15 03:00	-89 h
SARAL #674	07/11/15 18:02	H	04/11/15 23:30	G	05/11/15 06:00	-63 h

3.2 Coastal altimetry

In this paper, we used regional Mediterranean 1 Hz Jason-2 and SARAL Sea Level Anomaly (SLA), defined as the difference between the observed sea surface height and the mean sea level available and distributed by AVISO (User Handbook Ssalto/DUACS, 2016) as well as the experimental high frequency PEACHI (Prototype for Expertise on SARAL for Coastal, Hydrology and Ice) products (Valladeau et al., 2015.). Some specific retracking algorithms, corrections, editing procedures and MDT have been applied to these products and have been described below.

3.2.1 Retracking

One of the largest sources of errors in coastal altimetry is the inaccurate processing of the return waveforms. A significant number of ocean return waveforms near the coast indeed do not conform to the standard Brown model (Brown, 1997)), as they are affected by the noisier radar echoes from the land and/or calmer water contamination (Vignudelli et al., 2011). Several studies addressed this issue in the coastal domain.

For example, Brooks et al. (1998) analysed the TOPEX waveforms obtained when the altimeter transited from water to land and from land to water. They showed that waveform retracking can be used to extend the altimeter-derived sea surface topography several kilometres shoreward. Deng et al. (2002) investigated the behaviour of ERS-2 and POSEIDON altimeter waveform data in the Australian coastal region and mapped a boundary, located approximately 22 km from the coast of Australia, within which the altimeter range may be poorly estimated. Deng and Featherstone (2006) developed a retracking system that includes least-squares fitting of a five-parameter model and a threshold method applied to altimeter waveforms around Australia. In addition to the previously mentioned studies, Gomez-Enri et al. (2009) developed an experimental mixed Brown-specular retracker for the specular peak embedded within a Brown-type ocean waveform. More recently, new coastal retracking strategies have been developed and successfully applied, such as the ALES (Adaptive Leading Edge Subwaveform) (Passaro et al., 2014) and ALES+ (Passaro et al., 2018), potentially applicable to all pulse-limited altimetry missions over both open and coastal ocean with the same accuracy.

In this study, three types of retracking algorithms have been applied to PEACHI products. Their main characteristics are described below:

i. Red3 PISTACH (Prototype Innovant de Système de Traitement pour les Applications Côtières et l'Hydrologie) (Coastal and Hydrology Altimetry product handbook, 2010): This algorithm selects an analysis window centred on the main leading edge of the waveform and retracking parameters in this reduced window [-10; +20 samples] with a Maximum

Likelihood Estimator solving for 3 parameters (range, amplitude and Sigma composite).

ii. MLE4 (Maximum Likelihood Estimator) (Amarouche et al., 2004): This algorithm is an evolution of the Red3 retracker but is optimised for coastal applications with the estimator that solves for 4 parameters, adding the slope of the waveform trailing edge with respect to the Red3.

iii. Adaptive (Poisson et al., 2018): This approach is based on a physical retracking model accounting for the mean square slope of the surface. It grants the model the capability to adapt from a diffuse waveform to a pure specular waveform. The model accounts for instrumental characteristics (point target response, Antenna Gain Pattern, etc.) and a numerical solution can be used. The fitting criterion used is a pure least square only if the waveform classification performed before the fitting identifies a peaky waveform.

For AVISO products, the performance of MLE3 retracking (Amarouche et al., 2004) has been assessed. This retracking is similar to that for MLE4 but fits three unknown parameters (amplitude, arrival time and rise time) while the fourth, the trailing edge decay, is held fixed.

3.2.2 Geophysical Corrections

In addition to waveform retracking, other sources of uncertainties arise from the application of geophysical corrections to the altimetric sea surface height (SSH), defined as the height measured with respect to an arbitrary reference level, called the reference ellipsoid, which is not always optimised for the coastal domain. The main corrections used in this paper are listed in Table 2 and described in the following sections.

One of the most critical corrections is the wet tropospheric path delay, showing a standard error of +/- 3 cm in the coastal domain (Smith et al., 2008). Approaching the coast, wet tropospheric signals have a smaller space-temporal scale of variability, which are poorly resolved by numerical models or are less precisely estimated by on-board radiometer, the radiometric footprint being potentially corrupted by land contaminations. Until recently, most altimeter data in a 10–30 km coastal band of the NWMed were flagged as invalid and discarded from standard regional products (Bouffard, 2007; Bouffard et al., 2008a, 2008b). The regional AVISO products used in this study contain an enhanced wet tropospheric correction near the coast (more details in Brown, 2010). The same approach has been applied to Jason-2 PEACHI products (Valladeau et al., 2015). For SARAL PEACHI products, the method described in Valladeau et al. (2015) has been applied, whereby the last valid brightness temperature (BT) is extrapolated and considered in place of the contaminated BT as input to the computation of the WTC – an approach that is less accurate than the Brown (2010) method but much simpler to configure and implement.

Although several algorithms for improving the wet path delay near the coast have been developed recently (Cipollini et al., 2017; Desportes et al., 2010; Fernandes et al., 2015; Fernandes and Lázaro, 2016), the detailed evaluation of related improvements do not lie within the scope of the present paper, which mainly focuses on the impact assessment of applying coastal-oriented retracking, editing and high-resolution MDT.

Both AVISO and PEACHI products use the Dry Tropospheric correction computed from 6-hour span outputs from the ECMWF (European Centre for Medium-Range Weather Forecasts) model. The dry tropospheric correction has a maximum standard error of +/- 1–2 cm in the coastal domain (Smith et al., 2008).

For AVISO, the GOT4.8 (Ray, 2013) ocean tide solutions were applied, while the FES2012 was used for PEACHI (Carrere et al., 2012), despite the tide signals (and associated error) in the considered region being particularly low (Alberola et al., 1995).

With regard to the SSB, a 2D wind speed model as a function of backscatter and Significant Wave Height (SWH) was developed in the framework of the PEACHI project (Valladeau et al., 2015), while an empirical solution fitted on six months of SARAL GDR_C data (from NOAA Laboratory for Satellite Altimetry) was used in AVISO products (User Handbook Ssalto/DUACS, 2016). Alternative sea state bias (SSB) solutions are available in literature (Tran et al., 2010; Pires et al., 2016), aimed at developing a finer modelling of this effect, but have not been assessed in this study. The accuracy of SSB is about 2 cm (Smith et al., 2008).

In addition to the previously mentioned correction, the Global Ionospheric Map (GIM) from JPL (Jet Propulsion Laboratory) has been considered for the ionosphere correction for both AVISO and PEACHI products. Although the most accurate way to model the ionospheric effect is by using dual-frequency measurements (like in Imel, 1994), this approach is not applicable to SARAL, as it is a monoband radar altimeter. Thus, the JPL GIM model has been adopted in this study, as it is applicable to both Jason-2 and SARAL. The ionospheric correction has an error budget of +/- 3 cm on derived SSH (Callahan, 1984). Both PEACHI and AVISO products are provided including a so-called Dynamic Atmospheric Correction (DAC) (Carrère and Lyard, 2003).

3.2.3 Coastal Editing Strategy

As the PEACHI experimental products have a high rate sampling of 40Hz for SARAL and 20Hz for Jason-2, specific editing and filtering procedures have been developed, following methods described in Bouffard et al. (2010). Figure 2 depicts an example of this procedure applied on AltiKa track #429 in deriving the edited (red curve) and filtered (green curve) heights from the raw data (blue curve).

First, a ten-step recurrent 2*std editing algorithm was developed and applied to corrected high-rate along-track PEACHI SLA in order to remove residual spikes (see red curve on Figure 2). For each iteration, first, the difference between the altimetry raw and smoothed data was computed and then spikes higher than two standard deviations are flagged, removed and replaced by linearly interpolated values. The next iteration begins from this result by performing the spikes filtering and smoothing again. This recurrent procedure is repeated ten times in order to obtain the final edited and filtered SLA. At the end of these editing steps, 4% of spikes were eliminated from SARAL track #429 and 12% from SARAL track #674, while 7% spikes were filtered out from Jason-2 track #9. Thereafter, the edited high rate altimetric SLA was low-pass filtered (using a moving average filter) with a window of 2.5 km for SARAL (see green curve on Figure 2) and 8.5 km for Jason-2 in order to reduce residual noise, as in Bouffard et al. (2010). The MVP derived currents and ADCP currents were also smoothed from the raw signal with the same filter. Figure 2 also shows (in black) the 1 Hz AVISO product, highlighting the differences with respect to high-rate PEACHI products in terms of SLA-observed features.

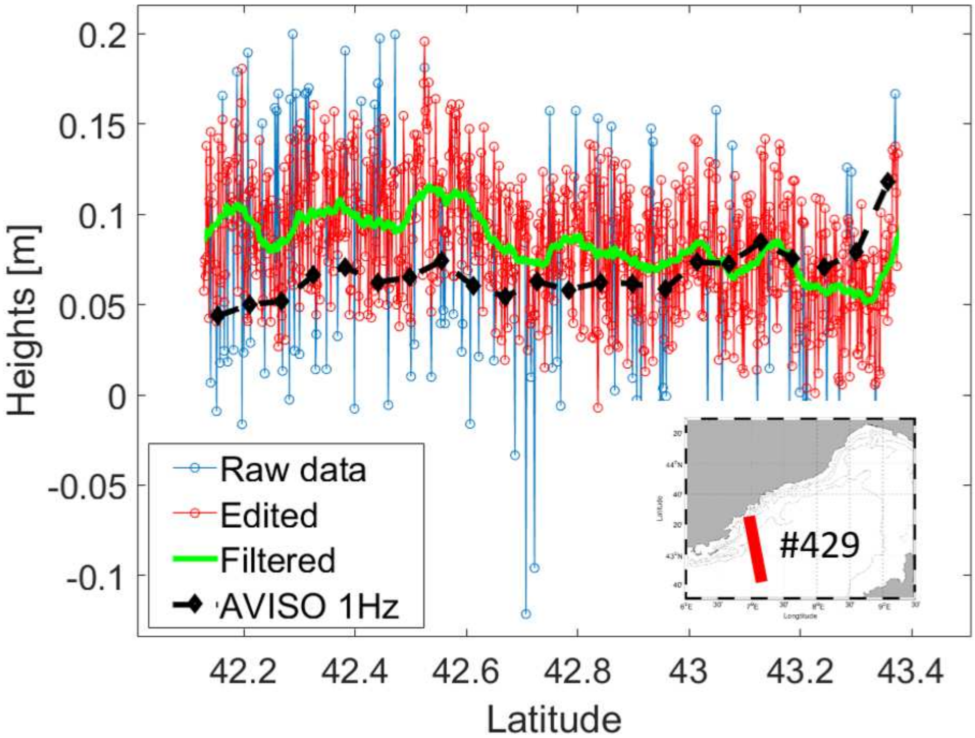

Figure 2 PEACHI high rate altimetry SLA editing and filtering for SARAL track #429. The black line corresponds to the AVISO 1 Hz track.

3.2.4 Mean Dynamic Topography (MDT)

The AVISO and PEACHI absolute geostrophic currents were then calculated from the ADT, using the Powell and Leben (2004) filtering with a cut-off distance of 15 km, roughly corresponding to the local Rossby radius of deformation over the study area (Grilli and Pinardi, 1998). Two Mean Dynamic Topography (MDT) have been considered, spatially interpolated and added to the altimetric SLA in order to obtain the along-track ADT: the Rio "old" MDT (after RIO07), resolution 1/8º (Rio et al., 2007; see Figure 3a) and the Rio "new" MDT (RIO14) with resolution 1/16º (Rio et al., 2014; see Figure 3b).

A linear interpolation was applied to both RIO07 and RIO14 gridded MDTs to obtain an along-track MDT to be added to the altimetry SLA measurements.

The RIO14 benefits from the improvements enabled by the use of extended data sets and refined processing techniques. The updated data set spans the 1993–2012 period and consists of drifter velocities, altimetry data, hydrological profiles and model data. The methodology is similar to the previous RIO07, which did not use any hydrological profiles. As compared to the RIO07, the RIO14 therefore features shorter-scale structures owing to the use of more *in situ* and satellite-based observations.

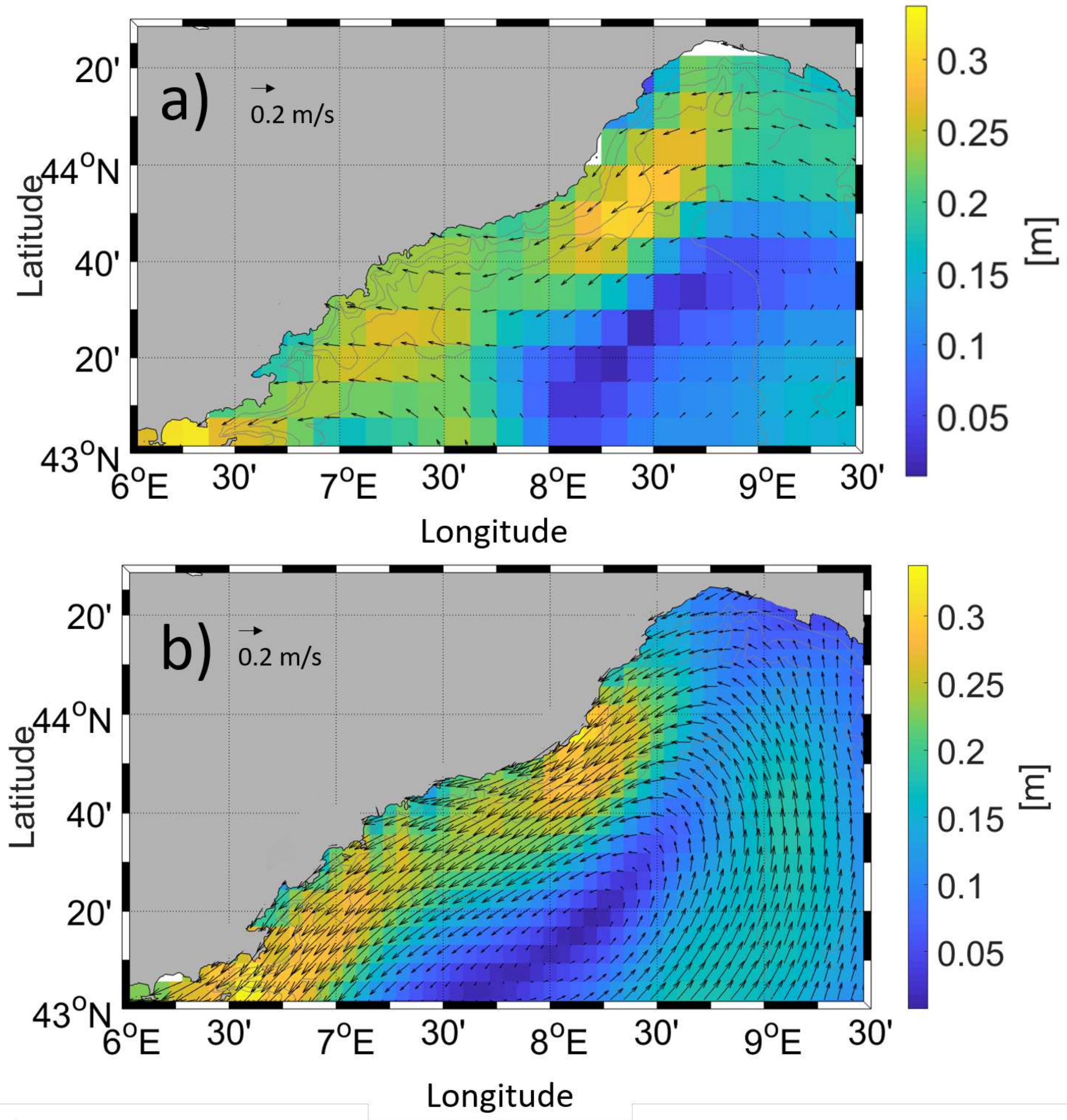

Figure 3 RIO07 (a) and RIO14 (b) MDT overlapped by the derived mean current.

Table 2 Altimetry data characteristics

<table>
<tr><th>SLA</th><th>MDT</th><th>Retracker</th><th>Sampling</th><th>SLA Coastal Editing</th><th>Spatial Filtering</th><th>Corrections</th></tr>
<tr><td>AVISO Jason-2</td><td>RIO14 RIO07</td><td rowspan="2">MLE3</td><td rowspan="2">1 Hz</td><td rowspan="2">No</td><td rowspan="2">No</td><td rowspan="2">Wet tropo (Brown, 2010)
Dry tropo (ECMWF Model)
Ionospheric (GIM from JPL)
Tides (GOT4.8 (Ray, 2013)
SSB (User Handbook Ssalto/DUACS, 2016)
DAC (Carrère and Lyard, 2003)</td></tr>
<tr><td>AVISO SARAL</td><td>RIO14 RIO07</td></tr>
<tr><td>PEACHI Jason-2</td><td>RIO14 RIO07</td><td rowspan="2">Red3 MLE4 Adaptive</td><td>20 Hz</td><td>10-step recurrent algorithm (Bouffard et al., 2010)</td><td>8.5 Km</td><td rowspan="2">Wet tropo (Brown, 2010 for Jason-2 and Valladeau et al., 2015 for SARAL)
Dry tropo (ECMWF Model)
Ionospheric (GIM from JPL)
Tides (FES2012 (Carrere et al., 2012))
SSB (Valladeau et al., 2015)
DAC (Carrère and Lyard, 2003)</td></tr>
<tr><td>PEACHI SARAL</td><td>RIO14 RIO07</td><td>40 Hz</td><td>10-step recurrent algorithm (Bouffard et al., 2010)</td><td>2.5 Km</td></tr>
</table>

4 Results and discussions

4.1 Impact of *in situ* MVP reference depth and sinopticity issue

As reported in section 3.1, temperature, salinity and density fields retrieved by MVP can be used to estimate DH with respect to an arbitrary reference depth, which is supposed to be a no-motion level. As the reference depth issue does not affect altimetry, a sensitivity study has been performed to highlight effects on the computation of MVP-derived surface geostrophic current when compared to altimetry (shown in Figure 4). The latter shows the different MVP-derived geostrophic currents computed by varying the reference depth, compared with PEACHI geostrophic currents using the MLE4 retracker. Each of the four transects has a different maximum depth for which valid measurements are available: 293 m for transect A – B, 330 m for transect D – A, 321 m for transect G – I and 278 m for transect H – G. Figure 5 reports the mean and standard deviation of the differences between PEACHI and MVP at different reference depths.

Examining the comparison statistics reported in Figure 5, it can be seen that the differences are reduced between altimetry and MVP datasets for transect D – A and H – G when considering a deeper reference level. For transect H – G, the difference between the two sensors is reduced from 0.052 m/s for a reference depth of 90 m to 0.028 m/s for a reference depth of 278 m. The same conclusion is obtained for transect D – A and transect A – B with a mean reduction from 0.092 m/s to 0.041 m/s and from 0.210 m/s to 0.178 m/s, respectively. This is potentially caused by the deep flow of the NC along the Ligurian continental slope. The vertical temperature profile shows the NC signature with a stronger temperature up to a depth of 90 m for latitudes higher than 43.35º (see Figure 10 and associated discussions).

The results obtained for the MVP transects out of the NC are different. For transect G – I, the mean reduction of altimetry and MVP current difference is observed up to a 140-m depth, whereas the differences go up for a higher depth (as for surface layers). This pattern could be potentially linked to the sub-surface currents associated with a strong and rapidly evolving mesoscale feature intercepted by this transect but not seen by transect H – G. Transects G – I and H – G are almost collocated but have a time separation of about one day (see Table 2) during which dynamical conditions may have changed with fine-scale surface features having moved in between the two MVP passes. This is confirmed by examining the vertical temperature profiles on which changes are clearly observed along the water column (see Figure 10 and associated discussions). These high-frequency variations cannot be observed by instantaneous altimetry measurements, while they affect the MVP measurements all along the data sampling, emphasising potential impacts of synoptic issues in altimetric versus *in situ* comparisons.

According to the above results (also confirmed by using Red3 or Adaptive retrackers in the sensitivity study) and despite the spotted sinopticity issue, the agreement between altimetry and MVP is generally satisfying when considering the deepest reference level (different for each of the four considered transect) as well as 20–30 km offshore (the grey square on Figure 4). On one hand, the deepest reference level has been kept for the remaining analyses and is the one adopted in the results presented in section 4.3 On the other hand, two alternative retrackers (Red3, Adaptive) have been used and evaluated to highlight the potential improvement in the 20–30 coastal bands.

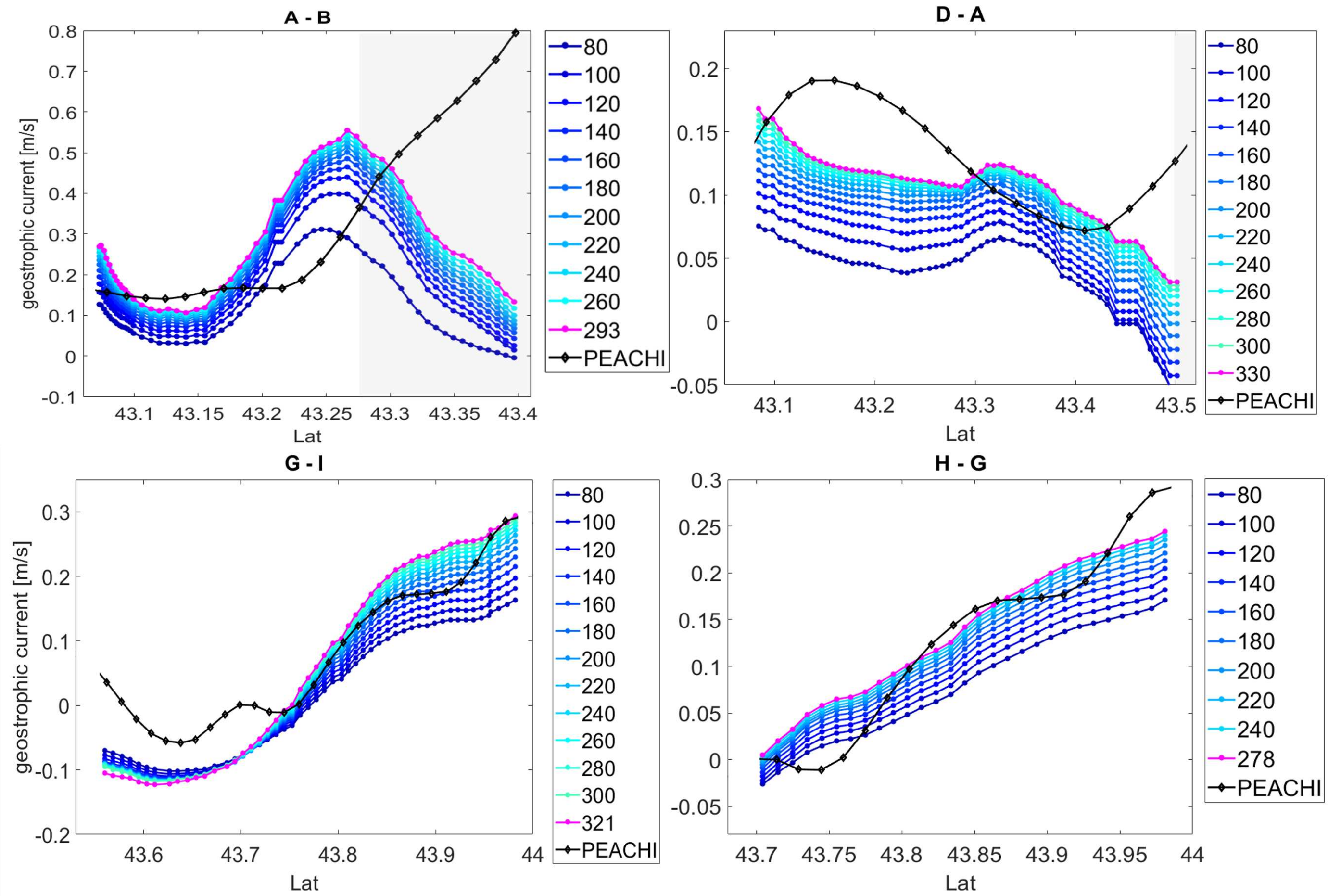

Figure 4 Reference depth sensitivity study for transects A – B, D – A, G – I and H – G. Different colours are associated with different reference depths (in meters) considered in the vertical integration of MVP data while the PEACHI altimetry data (MLE4 retracker) are shown in black. The magenta line represents the MVP derived currents at the maximum operating depth. The shaded grey areas in transects A – B and D – A correspond to 20 km from the coast.

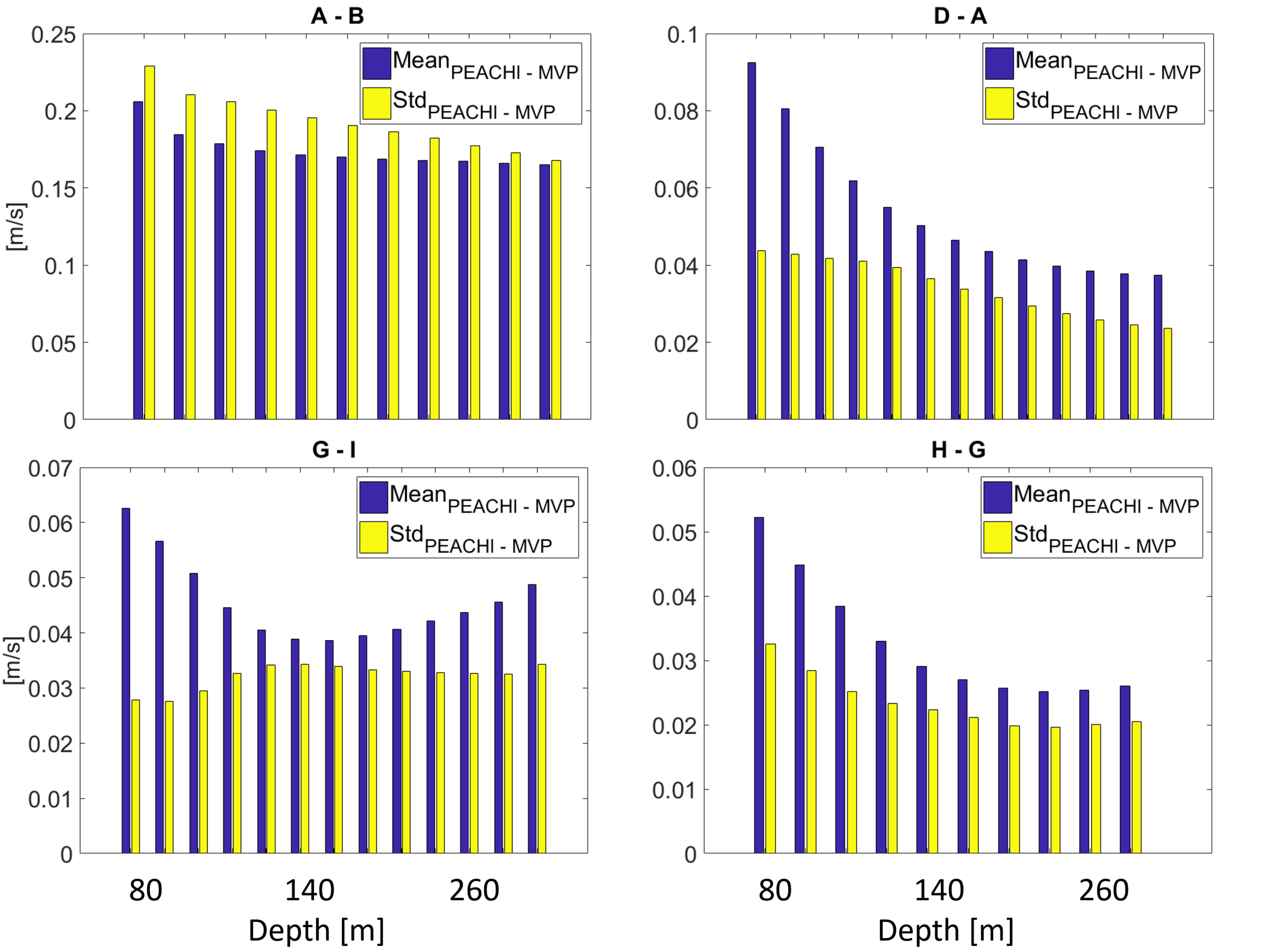

Figure 5 Mean (blue) and standard deviation (yellow) of the current differences between PEACHI and MVP.

4.2 Impact of physical content and reference depth

In order to assess the potential impact of the reference depth on the MVP retrieved current, geographical plots of the differences of the surface across-track current ADCP-MVP (coloured dots) have been computed (Figure 6), superposed to the cross-track component of the deep ADCP current, measured at 270 m depth. Comparison between surface across track MVP and ADCP derived currents are shown in Figure 7 for each of the cruise transects.

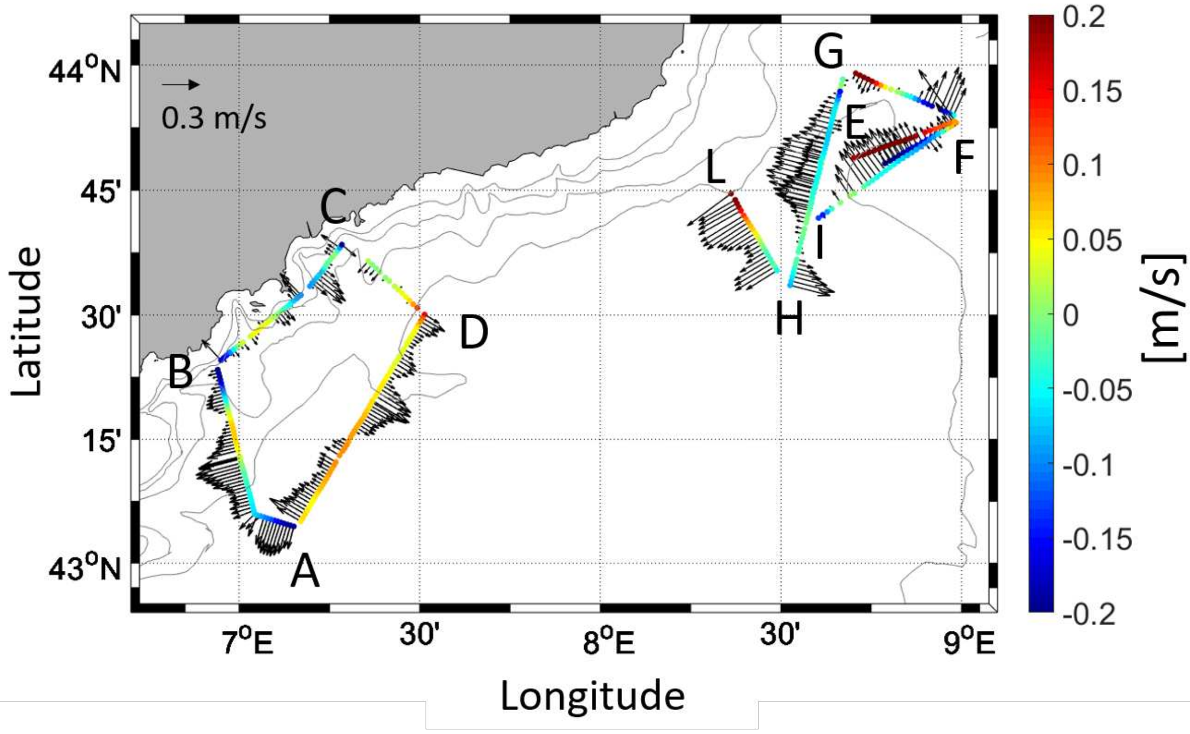

Figure 6 Geographical plot of the differences (coloured dots) of the surface across track current ADCP-MVP. The vectors are related to the cross-track component of the ADCP current at 270 m depth.

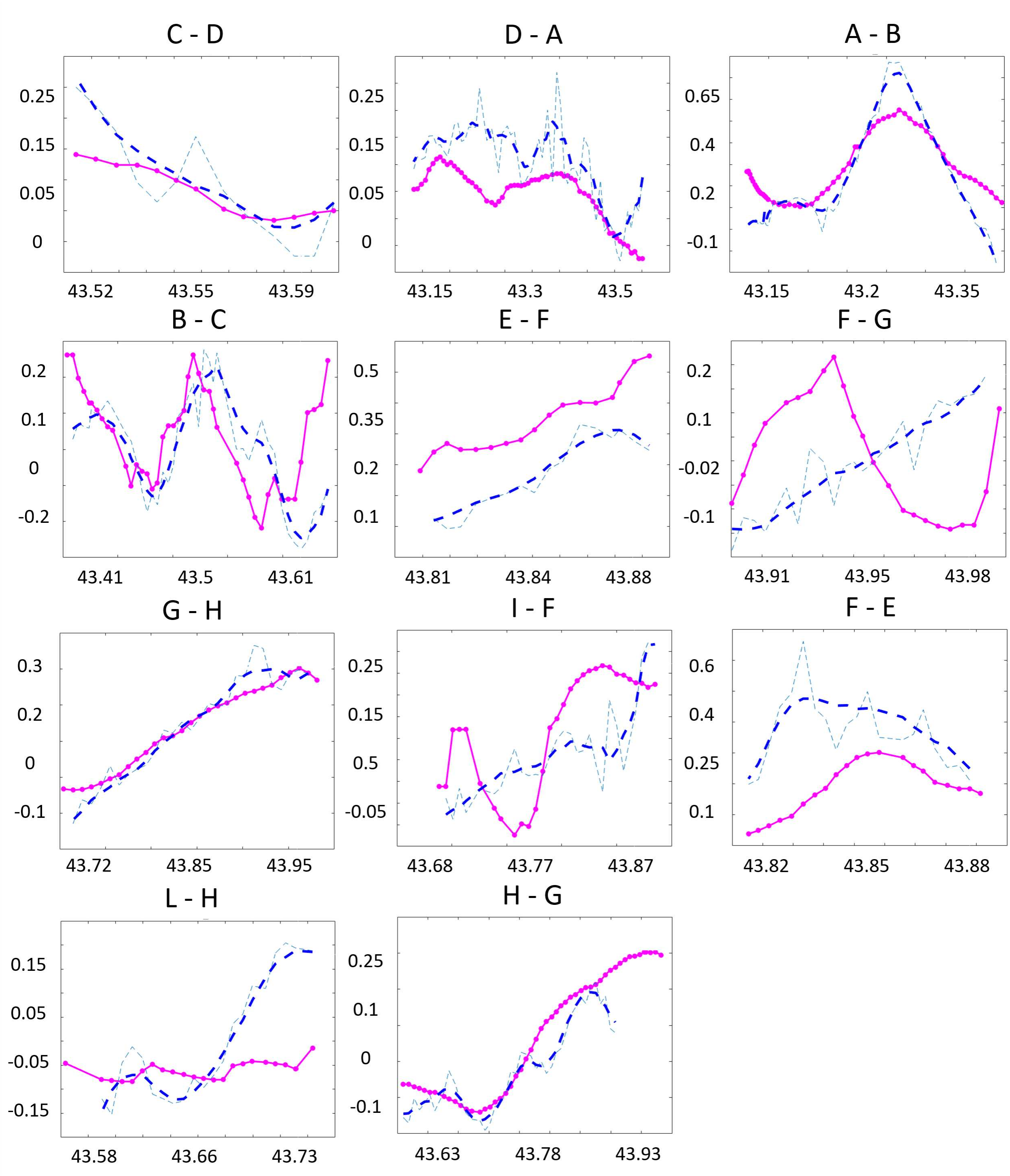

Figure 7 Comparison between MVP (magenta) and ADCP currents (m/s) vs. Latitude (raw data in thin blue, filtered and smoothed data in dashed thick blue) for each transect.

The principal differences between the two *in situ* observing systems highlighted in Figure 7 should be mainly related to the fact that ADCP measures the total absolute current and contains both geostrophic and ageostrophic motion, while the MVP measurements are referenced to an unknown no-motion level and – as altimetry – capture the single geostrophic component.

Figure 6 shows that if a strong deep current is present at 270 m, the no-motion hypothesis is not verified, which consequently creates inconsistencies when comparing DH-derived MVP currents with the ones from ADCP (and hence with altimetry). This is evident from transect F – G, E – F and F – E, where the differences between the two observing systems are particularly high (> 0.16 ms^{-1}). This is also valid when examining transect A – B, where a strong deep current is visible in Figure 6, generating a difference of 0.10 ms^{-1} between surface MVP and ADCP currents. On the other hand, transects G – H and H – G show small differences and high correlation (> 0.95), although the ADCP measurements show finer-scale dynamics, perhaps due to ageostrophic variations that occurred during the time of route H – G and not during the same geographical transect G – H. During the period from October 30 to November 2, 2015, a strong north-easterly wind event with velocity up to 70 km h^{-1} was recorded over the whole area (Marrec et al., 2018), reinforcing high-frequency and small-scale features

In addition, looking at *in situ* comparison statistics (Table 3), anticorrelated value was found for transect F – G as well as significant differences for transects E – F, F – E and F – G. Moreover, ADCP observations on Figure 7 show small-scale dynamics, not depicted by altimetry and MVP (for example along the transect D – A), but attesting the presence of high-frequency ageostrophic likely variations.

Table 3 MVP vs ADCP Comparison statistics. For correlation results the level of significance is 95%

Transect	Mean(ADCP-MVP) [m]	Std(ADCP-MVP) [m]	Mean(MVP) [m]	Std(MVP) [m]	Mean(ADCP) [m]	Std(ADCP) [m]	Corr(ADCP, MVP)
C - D	0.03	0.04	0.08	0.04	0.11	0.08	0.94
D - A	0.06	0.03	0.10	0.05	0.16	0.06	0.81
A - B	0.10	0.08	0.27	0.14	0.23	0.24	0.93
B - C	0.13	0.13	0.03	0.10	0.00	0.13	0.44
E - F	0.18	0.05	0.34	0.11	0.18	0.11	0.89
F - G	0.18	0.07	0.01	0.12	0.00	0.10	-0.59
G - H	0.03	0.02	0.14	0.12	0.14	0.14	0.99
I - F	0.12	0.06	0.12	0.14	0.07	0.10	0.51
F - E	0.20	0.09	0.19	0.08	0.38	0.08	0.44
L - H	0.08	0.08	-0.06	0.02	-0.01	0.12	0.72
H - G	0.05	0.04	0.08	0.16	-0.02	0.12	0.95

After geostrophy, one of the major contributions to the ocean surface currents is the Ekman response of the ocean to high-frequency wind stress. Various studies have focused on understanding and modelling these currents in a more effective and comprehensive manner (Ralph and Niiler, 1999; Lagerloef et al., 1999; Elipot and Gille, 2009; Rio et al., 2003, 2011, 2012). The potential impacts of ageostrophy signatures from Ekman have been tentatively assessed in this study using GlobCurrent version 2 Ekman current at 0.25° resolution, 3-hourly, available from 2002 to 2014 (accessed from http://www.globcurrent.org/). However, due to the coarse resolution of the GlobCurrent products and a lack of coverage over the coastal domain, it was not possible to assess precise Ekman impacts on the study area. A product with finer resolution should be processed in future GlobCurrent versions but was not available at the time of this study.

The following section reports the comparison between satellite altimetry and MVP with particular emphasis on the impacts of altimetry processing.

4.3 Impact of altimetry processing

SARAL tracks #429 and #674 together with Jason-2 track #9 SLA, ADT and derived currents were compared to MVP geo-located measurements (Figure 8). Tables 4 and 5 report the mean statistical scores per mission. In total, combinations of 12 comparisons per track have been performed between satellite altimetry measurements (considering different products, MDT and corrections) and *in situ* MVP/ADCP transects. The analysis has been performed up to 14.5 km from the coast for SARAL track #429, 37 km for SARAL track #674 and up to 13 km for Jason-2 track #9.

Examining the comparison plots between Jason-2 track #9 and MVP transect A-D (Figure 8a), it can be seen that the two bumps visible in currents at Latitude 43.2°and 43.4° are related to the interception of the NC, which intersects the altimetric track twice due to its orientation with respect to the main flow. The NC signature is also evident when looking at SARAL track #429 from which the main current peak of 0.55 m/s at Latitude 43.25° is captured by MVP and ADCP measurements (Figure 8b). Along the SARAL track #674 and *in situ* transects G – I and H – G, a dipole-like mesoscale structure is observed in each altimetric dataset (see section 4.4; Figures 8c and 8d).

Despite good general agreement between altimetry and MVP, some important discrepancies were also observed. For track #429, the mean difference with respect to the MVP and ADCP current are 0.08 m/s and 0.20 m/s, respectively. These significant differences might potentially be due to land contamination affecting altimetry measurements approaching the coast and not processed with optimal retracking and/or local corrections. MVP and ADCP show some disagreements along the transect A – D, whereas ADCP – not affected by reference level issue – and altimetry (track #9) show quite a similar pattern with an increasing velocity when approaching the coastline.

When compared to ADCP and MVP-derived current, the benefit of adding MDT to the altimetric SLA is obviously confirmed for all considered tracks and missions; this is particularly evident for SARAL tracks, for which an improvement of 30% in correlation was observed. When compared to the RIO07 MDT, the use of the RIO14 further improves the comparison scores in terms of correlation between altimetry data and MVP, with a mean increase of 10% for both AVISO and PEACHI products (Tables 4 and 5).

Using the PEACHI products, the mean and standard deviation differences between MVP and altimetry are still reduced: the overall mean difference goes from 0.04 m/s to 0.02 m/s for SARAL and from 0.35 m/s to 0.26 m/s for Jason-2 for 1 Hz AVISO and PEACHI products respectively. Comparison statistics (Table 4) show that for PEACHI products, the adaptive retracker provides better performances in coastal regions (correlation > 0.9) for both 40 Hz SARAL and 20 Hz Jason-2 sensors when compared to standard 1 Hz regional AVISO.

With regard to previous studies (Birol et al., 2015; Verron et al., 2015; Troupin et al., 2015), considering AltiKa sensor on-board, SARAL provides better statistical agreement with *in situ* than the Ku-band mission, such as Jason-2 and, particularly in this study, using the combination with RIO14 and adaptive retracking, confirming that the Ka band is more reliable in resolving fine-scale coastal dynamics.

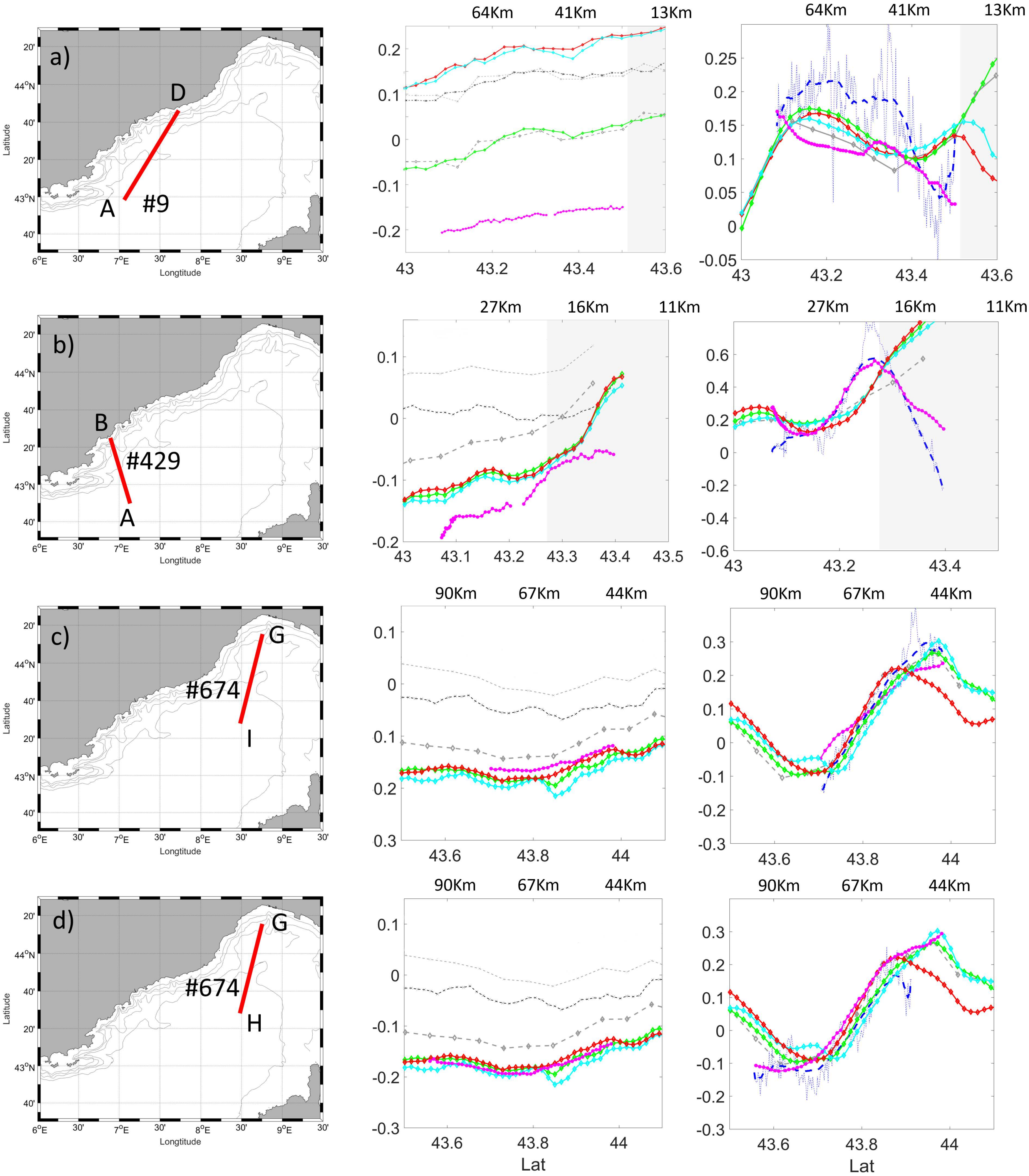

Figure 8 PEACHI Altimetry (grey for SLA+RIO07 and red for adaptive retracking, cyan for Red3 retracking and green for MLE4 retracking for SLA+RIO14) vs AVISO altimetry (light grey for SLA+RIO07 and grey for SLA+RIO14) vs *in situ* (magenta for MVP, blue for ADCP). The different markers used for both AVISO and PEACHI altimetry are related to elevations and currents computed with a different MDT (crosses for RIO07

and diamonds for RIO14). First column reports track geolocation, second column reports ADTs (m) vs Latitude and third column reports satellite across track current (ms-1) derived from ADT computed only adding RIO14 to SLA vs Latitude together with in situ derived current vs Latitude. The distance to the coast is also reported in kilometres.

Table 4 PEACHI ADT and V vs MVP average comparison statistics (correlation) per retracking method (the level of significance is 95%)

Satellite	MDT	Parameter	Adaptive	MLE4	RED3	Total Average per MDT
SARAL	RIO14	ADT	0.93	0.90	0.78	0.87
		V	0.75	0.67	0.79	0.74
	RIO07	ADT	0.58	0.55	0.30	0.48
		V	0.76	0.51	0.71	0.66
	Total Average per Retracking	ADT	0.75	0.72	0.54	0.67
		V	0.76	0.59	0.75	0.70
Jason-2	RIO14	ADT	0.92	0.91	0.77	0.87
		V	0.71	0.74	0.73	0.73
	RIO07	ADT	0.83	0.81	0.71	0.79
		V	0.70	0.74	0.72	0.72
	Total Average per Retracking	ADT	0.88	0.86	0.74	0.83
		V	0.71	0.74	0.73	0.72

Table 5 AVISO ADT and V vs MVP average comparison statistics (correlation) per retracking method (the level of significance is 95%)

Satellite	MDT	Parameter	MLE3
SARAL	RIO14	ADT	0.86
		V	0.82
	RIO07	ADT	0.60
		V	0.76
	Total Average per Retracking	ADT	0.73
		V	0.79
Jason-2	RIO14	ADT	0.87
		V	0.71
	RIO07	ADT	0.70
		V	0.68
	Total Average per Retracking	ADT	0.79
		V	0.70

From a general point of view, the comparison between altimetry and MVP over the study area is improved when considering experimental PEACHI high-rate altimetry data rather than the Mediterranean regional AVISO products. The NC signatures and small-scale oceanic features are, however, well captured by both datasets. Despite this encouraging result and as testified by cross-comparisons with collocated ADCP transects, the MVP measurements cannot be considered as a perfect reference dataset for validating coastal altimetry. This is due to its sensitivity to the reference level with regard to determining the DH along with the highlighted sinopticity issues induced by high frequency and partially ageostrophic small-scale dynamics occurring during data acquisition.

4.4 Observed circulation patterns

As shown on Figure 9, the combined use of surface altimetry and sub-surface *in situ* measurements (MVP and ADCP) allows the observation of small scale and coastal hydrodynamic features that are consistent with frontal structures depicted by PODAAC Sea Surface Temperature data (SST, L4 data, JPL OurOcean Project, 2010).

In Figure 9, looking at transect A – B, the NC main path, with high current velocity (> 0.3 ms^{-1}) is intercepted by altimetry around Latitude 43.25º and 6.8º Longitude. The associated surface frontal structure is also clearly captured by ADCP and MVP-derived current as well as from remote-sensing SST image. There, the vertical structure is characterised by the temperature profile of MVP, with higher temperature > 18 °C (Figure 10) caused by the NC main flow and depicted up to its maximum depth (80 m).

More East and offshore, an eddy-like structure is instead depicted at the surface by altimetry, ADCP and MVP-derived currents along the transect G – I. Along the same transect, satellite SST also shows a zone of low temperature with values below 17 °C. This zone is surrounded by warmer boundary waters characterised by SST higher than 17 °C, suggesting ascendant vertical pumping of cold water in the central part of this small-scale dynamical feature.

Both *in situ* and satellite-derived surface current directions indicate that this mesoscale feature is linked to a cyclonic recirculation of the NC in the Ligurian sub-basin. Marrec et al. (2018) reported on this event, also attributing the important role of Ekman pumping, induced by a strong wind event just before the OSCAHR cruise, which has an impact on ocean biogeochemistry. Besides the strong wind event occurring during the first day of the cruise, the region has experienced several wind events two weeks before the cruise (Marrec et al., 2018), inducing a strong decline in SST. The low temperature patch described by satellite SST and MVP profile supports the Ekman pumping hypothesis. This process was also important in fertilizing the upper layer with nutrient-rich upwelled waters.

Figure 10 depicts the salinity and temperature vertical sections of MVP transects A – B, G – I, H – G and D – A. In transect G – I, the sea surface salinity (SSS) was lower (< 38.20) in the cold core than in the warm boundaries (> 38.20) and salinity at 300 m in depth was higher than 38.50. A subsurface layer of low-salinity waters (< 38.10) is present with a 40 to 80 m thickness. This subsurface layer was observed up to the surface in the centre of the cold core (between Latitude 43.7º and Latitude 43.8º), whereas in warm boundaries, saltier (> 35.20) surface waters overlaid it. Low-salinity waters (< 38.10) at the surface of the cold patch support the vertical Ekman pumping hypothesis, as suggested from multi-sensor surface observations reported in Figure 9.

Transect H – G presents a lower salinity band (< 38.10) between 40 m to 80 m but without reaching the surface, as for transect G – I. Higher values of depth salinity are confirmed also for this transect. On transect A – B, where the signature of the NC is clearly visible from the temperature profile (Figure 10) and altimetric-derived current (Figure 9), the salinity values present lower values between 40 and 50 m depth in the Latitude range between 43.1º and 43.2º to reach a thickness of 100 m (i.e. from 50 m to 150 m) from Latitude 43.3º and Latitude 43.5º. The same features are observed in transect D – A, but the lower values of salinity reach a depth of 100 m.

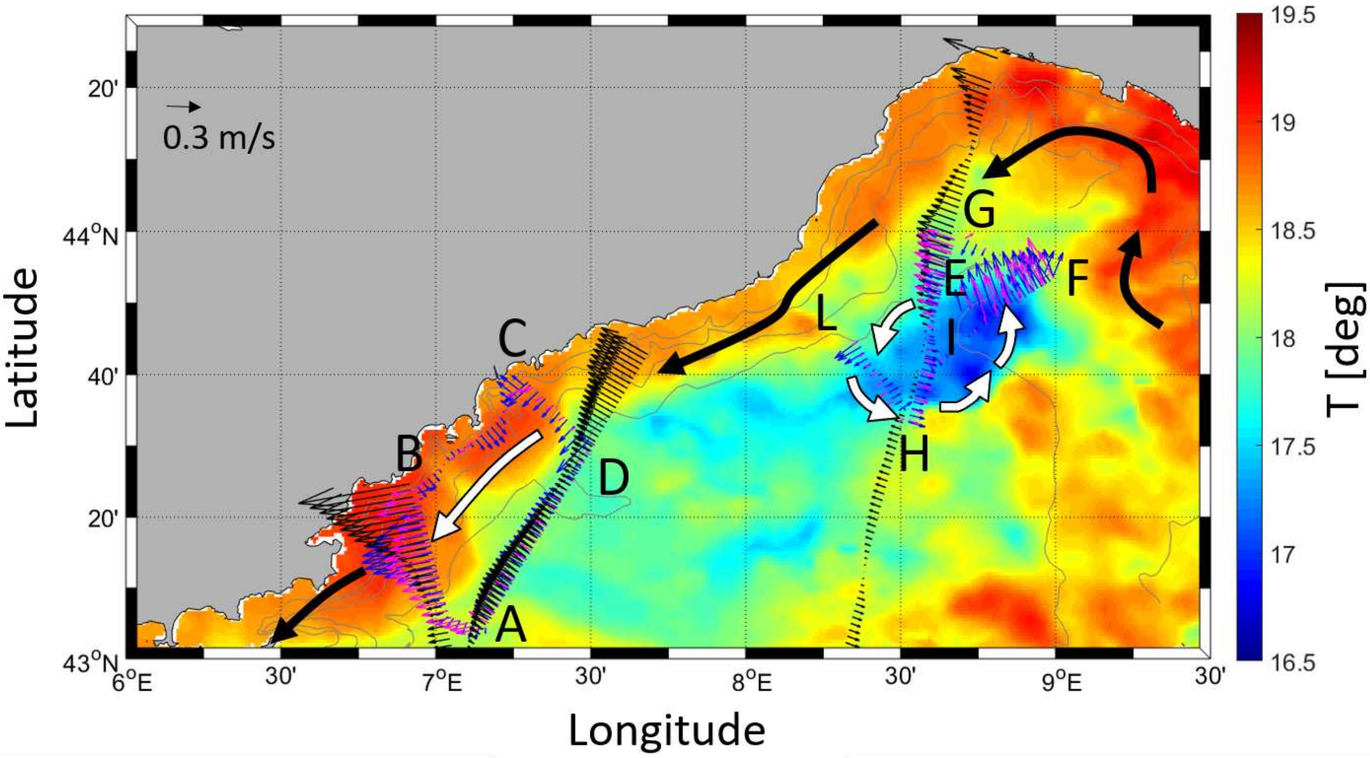

Figure 9 Surface circulation pattern derived from *in situ* (magenta for MVP and blue for ADCP) and PEACHI altimetry data (black). SST data is also shown with a Spatial Resolution of 0.062º (Latitude) x 0.062º (Longitude) and temporal resolution of 1 day. The SST maps is an average over the OSCAHR cruise time period October 29, 2015 to November 06, 2015). White arrows depict the surface oceanographic features reported also in Figure 10 vertical profiles.

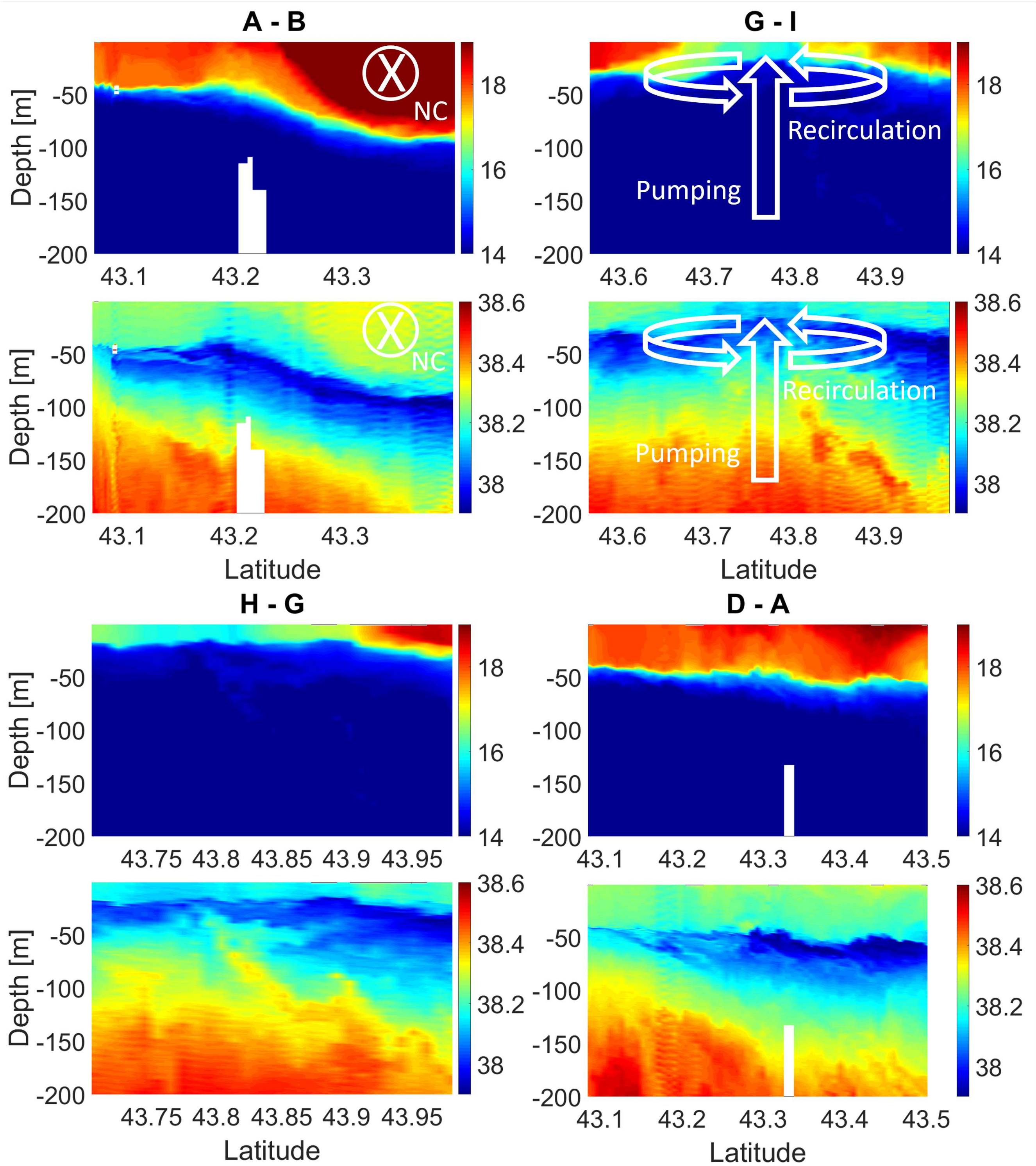

Figure 10 MVP Salinity and temperature vertical profiles. The oceanographic features have been depicted with white arrows.

5 Conclusions

The monitoring of small-scale processes in the coastal domain using satellite-based observations represents a key challenge in oceanography. In this paper, we discussed the issue of validating and optimising coastal altimetry data in areas characterised by fine-scale dynamics.

It has been discussed that regional 1 Hz altimetric data from AVISO are not always reliable close to the coast, and new experimental post processed and edited high rate PEACHI altimetric data have been considered to better resolve regional fine-scale features. Comparison statistics show that experimental high-rate PEACHI products using the adaptive retracker provide better performances in coastal regions for both 40 Hz SARAL and 20 Hz Jason-2 missions. Moreover, the use of the new RIO14 MDT instead of the RIO07 one increases the correlation scores with respect to *in situ* measurements.

The use of MVP platform has been assessed, as it was never used for validating coastal altimetry, highlighting the main challenges, advantages and limitations with respect to gliders. Further, regarding the MVP dataset, the importance of the reference level and sinopticity issues were discussed, and a sensitivity study was performed to highlight the effect on the derived geostrophic currents. It has been shown that, as for glider, measurements from the MVP are very promising for validating coastal altimetry techniques but cannot be considered as a perfect reference dataset by themselves. In this respect, the combined use of collocated MVP, altimetry and ADCP appears to be relevant, not only for validation purpose but also to better characterise the surface and sub-surface regional dynamics of the study area, including the North Current flow and the induced cyclonic recirculation in the eastern side of the Ligurian Sea. New benchmarking will also be performed, where the most recent developments in geophysical corrections and new retracking methods in coastal domains will be taken into consideration.

From a more general point of view, this study illustrated the complexity of setting up adequate *in situ* validation networks for coastal altimetry in areas dominated by geostrophic and ageostrophic fine-scale oceanographic processes. It confirmed the key importance of developing *ad-hoc* validation approaches using multiple types of collocated instruments, which allow diagnosing and understanding the physical content and mechanisms of the observed oceanic features. Recent (Sentinel-3) and future high-resolution topographic missions, such as Jason-CS, Sentinel-6 and SWOT, will continue to provide improved ocean parameters that can significantly help in understanding climate changes, coastal and (sub-)mesoscale dynamics. Their full exploitation and integration into re-analysis and forecasting system will however depend on our capability to continuously develop science-oriented diagnostics and uncertainty estimation. This objective can only be achieved through the deployment and maintenance of long-term, independent, fully characterised and traceable multi-sensor *in situ* observations (so-called "Fiducial Reference Measurements", FRM), collocated along altimetry tracks.

Acknowledgments

We would like to thank the DT-INSU people from la Seyne sur Mer and, in particular, Malika Oudia for her help in the administration work and Céline Heyndrickx and Frédéric Le Moal for their technical support. We would specially like to mention Genavir and Julien Fenouil for assisting us with the MVP.

MVP and the associated captors were brought by IFREMER and LOPB with co-funding by the Centre Européen de Technologies Sous-Marine (CETSM – Contrat de

Projet Etat Région 2007–2013 en PACA) and the French ANR FOCEA (project ANR-09-CEXC- 006-01 to M. Zhou and F. Carlotti). We would also like to extend our thanks to J. Thomas Farrar (MIT) for his suggestions on the cruise strategy. The OSCAHR cruise was supported by the MIO Axes Transverses" programme (AT-COUPLAGE), CHROME (PI M. Thyssen, funded by the Excellence Initiative of Aix-Marseille University – A*MIDEX, a French "Investissements d'Avenir" program), SeaQUEST (PI O. Ross, funded by the UE FP7 people), AMICO (PI C. Pinazo, funded by Copernicus – MEDDE French Ministery MDE), and BIOSWOT (PI F. d'Ovidio, funded by TOSCA/CNES). We also thank the captain and crew of the Téthys II research vessel. The project leading to this publication received funding from the European FEDER Fund under project 1166-39417. We are grateful for the support of Labex OT-Med (no. ANR-11-LABX-0061), funded by the French government through the A*MIDEX project (no. ANR-11-IDEX-0001-02).

The altimeter products were produced by Ssalto/Duacs and distributed by Aviso, with support from Cnes (http://www.aviso.altimetry.fr/duacs/)".

The Group for High Resolution Sea Surface Temperature (GHRSST) Multi-scale Ultra-high Resolution (MUR) SST data were obtained from the NASA EOSDIS Physical Oceanography Distributed Active Archive Center (PO.DAAC) at the Jet Propulsion Laboratory, Pasadena, CA (http://dx.doi.org/10.5067/GHGMR-4FJ01).

6 References

Alberola, C., Rousseau, S., Millot, C., Astraldi, M., Garcia- Lafuente, J.J., Gasparini, G.P., Send, U., Vangriesheim, A., 1995. Tidal currents in the Western Mediterranean Sea. Oceanol. Acta. 18(2), 273–284.

Aulicino, G., Cotroneo, Y., Ruiz, S., Sánchez Román, A., Pascual, A., Fusco, G. Budillon, G. 2018. Monitoring the Algerian Basin through glider observations, satellite altimetry and numerical simulations along a SARAL/AltiKa track. J. Mar. Syst. 179, 55–71. https://doi.org/10.1016/j.jmarsys.2017.11.006.

Amarouche, L., P. Thibaut, O.-Z. Zanife, J. P. Dumont, P. Vincent, N. Steunou, 2004. Improving the Jason-1 ground tracking to better account for attitude effects. Mar Geod. 27(1–2), 171–197.

Anzenhofer, M., Shum, C.K., Rentsh, M., 1999. Coastal altimetry and applications, Tech. Rep. 464, Geodedic Science and Survey, Ohio State University, Columbus.

Barrier, N., Petrenko, A., Ourmieres, Y., 2016. Strong intrusions of the Northern Mediterranean Current on the eastern Gulf of Lion: Insights from in-situ observations and high resolution numerical modelling. Ocean Dynamics, Springer Verlag. 66(3), 313–327.

Birol, F., Delebecque, C., 2014. Using high sampling rate (10/20 Hz) altimeter data for the observation of coastal surface currents: A case study over the Northwestern Mediterranean Sea. J. Mar. Syst. 129, 318–333, doi:10.1016/j.jmarsys.2013.07.009.

Birol, F., Niño, F., 2015. Ku and Ka-Band Altimeter Data in the Northwestern Mediterranean Sea. Mar. Geod. 38, 313–327, doi:10.1080/01490419.2015.1034814.

Birol, F., Cancet, M., Estournel, C., 2010. Aspects of the seasonal variability of the Northern Current (NW Mediterranean Sea) observed by altimetry. J. Mar. Syst. 81, 297–311. doi: 10.1016/j.jmarsys.2010.01.005.

Bonnefond, P., Laurain, O., Exertier, P., Boy, F., Guinle, T., Picot, N., Labroue, S., Raynal, M., Donlon, C., Féménias, P., Parrinello, T., Dinardo, S., 2018. Calibrating the SAR SSH of Sentinel-3A and CryoSat-2 over the Corsica Facilities. Remote Sensing. 10, 92.

Bouffard, J., S. Vignudelli, P. Cipollini, Menard, Y., 2008a. Exploiting the potential of an improved multimission altimetric data set over the coastal ocean. Geophys. Res. Lett. 35, L10601. doi: 10.1029/2008GL033488.

Bouffard, J., Vignudelli, S., Herrmann, M., Lyard, F., Marsaleix, P., Menard, Y., Cipollini, P., 2008b. Comparison of ocean dynamics with a regional circulation model and improved altimetry in the North-Western Mediterranean. Terrestrial Atmos. Oceanic Sci. 19.

Bouffard, J., F. Nencioli, R. Escudier, A. M. Doglioli, A. A. Petrenko, A. Pascual, P.-M. Poulain, Elhmaidi, D., 2014. Lagangian analysis of satellite-derived currents: Application to the North Western Mediterranean coastal dynamics. Adv. Space Res. 53, 788–801.

Bouffard, J., Naeije, M., Banks, C. J., Calafat, F. M., Cipollini, P., Snaith, H. M., Webb, E., Hall, A., Mannan, R., Féménias, P., Parrinello T., 2017. CryoSat ocean product quality status and future evolution. Adv. Space Res. https://doi.org/10.1016/j.asr.2017.11.043.

Bouffard, J., Roblou, L., Birol, F., Pascual, A., Fenoglio-Marc, L., Cancet, M., Morrow, R., Me´nard, Y., 2011. Introduction and assessment of improved coastal altimetry strategies: case study over the North Western Mediterranean Sea, in: Vignudelli, S., Kostianoy, A., Cipollini, P., Benveniste J. (Eds.), Coastal Altimetry. Springer, Berlin, Heidelberg, pp. 297–330.

Bouffard, J., Pascual, A., Ruiz, S., Faugère, Y., Tintoré, J., 2010. Coastal and mesoscale dynamics characterization using altimetry and gliders: A case study in the Balearic Sea. J. Geophys. Res. 115, C10029. https://doi.org/10.1029/2009JC006087.

Bouffard, J., Renault, L., Ruiz, S., Pascual, A., Dufau, C., Tintoré, J., 2012. Sub-surface small-scale eddy dynamics from multi-sensor observations and modelling. Prog. Oceanogr. 106, 62–79. ISSN 0079-6611. doi: 10.1016/j.pocean.2012.06.007.

Brooks, R.L, Lockwood, D.W., Lee, J.E., Hancock, D.W.I., Hayne, G.S., 1998. Land effects on Topex radar altimeter measurements in pacific rim coastal zones, in: Brown, R.A. (Ed.), Remote Sensing of the Pacific Ocean by Satellites. Earth Ocean & Space Pty. Ltd., Eveleigh, NSW, pp. 175–198.

Brown, G.S., 1997. The average impulse response of a rough surface and its applications. IEEE Trans. Antennas Propagation, AP-25. 67–74.

Brown, S., 2010. A novel near-land radiometer wet path-delay retrieval algorithm: Application to the Jason-2/OSTM advanced microwave radiometer. IEEE Trans Geosci. Remote Sens. 48(4), 1986.

Calafat, F.M., Cipollini, P., Bouffard, J., Snaith, H., Féménias, P., 2016. First evaluation of new CryoSat-2 products over the ocean. Remote Sens. Environ. 191, 131–144. doi: 10.1016/j.rse.2017.01.009.

Callahan, P. S., 1984. Ionospheric variations affecting altimeter measurements: A brief synopsis. Mar. Geod. 8, 249–263.

Carrère L., Lyard, F., 2003. Modeling the barotropic response of the global ocean to atmospheric wind and pressure forcing – comparisons with observations. Geophys. Res. Lett. 30(6), 1275. doi:10.1029/2002GL016473.

Carrere, L., Lyard, F., Cancet, M., Guillot, A., Roblou, L., 2012. FES 2012: A new global tidal model taking advantage of nearly 20 years of altimetry. Proc. 20 Years Altimetry, Venice, Italy.

Cipollini, P., Benveniste, J., Bouffard, J., Emery, W., Fenoglio-Marc, L., Gommenginger, C., Griffin, D.A., Hoyer, J., Kurapov, A., Madsen, K., Mercier, F., Millery L., Pascual, A., Ravichandran, M., Shillington, F., Snaith, H., Strub, P.T., Vandermark, D., Vignudelli, S., Wilkin, J., Woodworth, P., Zavala-Garay, J., 2009. The role of altimetry in coastal observing systems, in: Hall, J., Harrison, D.E., Stammer, D. (Eds.), Proceedings of OceanObs'09: Sustained Ocean Observations and Information for Society, Venice, Italy.

Cipollini, P., Benveniste, J., Birol, F., Fernandes, M. J., Obligis, E., Passaro, M. Strub, P. T., Valladeau, G., Vignudelli, S., Wilkin J., 2017. Satellite altimetry in coastal regions, in: Stammer, D., Cazenave, A. (Eds.), Satellite Altimetry Over Oceans and Land Surfaces, CRC Press, pp. 343–380. ISBN: 9781498743457.

Coastal and Hydrology Altimetry product (PISTACH) handbook, SALP-MU-P-OP-16031-CN 01/00, edition 1.0, October 2010.

Cyr, F., Tedetti, M., Besson, F., Beguery, L., Doglioli, A.M., Petrenko A.A., Goutx M., 2017. A new glider-compatible optical sensor for dissolved organic matter measurements: Test case from the NW Mediterranean Sea. Frontiers Mar. Sci. 4, 89. doi: 10.3389/fmars.2017.00089.

Declerck, A., Ourmières, Y., Molcard, A., 2016. Assessment of the coastal dynamics in a nested zoom and feedback on the boundary current: The North-Western Mediterranean Sea case. Ocean Dynam. 66, 1529–1542. doi: 10.1007/s10236-016-0985-4.

Deng, X., Featherstone, W., Hwang, C., 2002. Estimation of contamination of ERS-2 and POSEIDON satellite radar altimetry close to the coasts of Australia. Mar. Geod. 25, 249–271.

Deng, X, Featherstone, W.E., 2006. A coastal retracking system for satellite radar altimeter waveforms: Application to ERS-2 around Australia. J. Geophys. Res. 111, C06012. doi:10.1029/2005JC003039.

Desportes, C., Obligis, E., Eymard, L., 2010. One-dimensional variational retrieval of the wet tropospheric correction for altimetry in coastal regions. IEEE Trans. Geosci. Remote Sens. 48(3), 1001–1008.

Dinardo, S., Fenoglio, L., Buchhaupt, C., Becker, M., Scharroo, R., Joana F., Benveniste, J., 2017. Coastal SAR and PLRM altimetry in German Bight and West Baltic Sea. Adv. Space Res. 62(6), 1371–1404.

Doglioli A., 2015. Observing submesoscale coupling at high resolution, OSCAHR cruise, RV Téthys II, http://dx.doi.org/10.17600/15008800.

Elipot, S., Gille, S.T., 2009. Estimates of wind energy input to the Ekman layer in the Southern Ocean from surface drifter data. J. Geophys. Res. 114, C06003.

Fernandes, M.J., Lázaro, C., Ablain, M., Pires, N., 2015. Improved wet path delays for all ESA and reference altimetric missions. Remote Sens. Environ. 169, 50–74.

Fernandes M.J., Lázaro, C., 2016. GPD+ wet tropospheric corrections for CryoSat-2 and GFO altimetry missions. Remote Sens. 8(10), 851.

Forget, P., Saillard, M., Broche, P., 2006. Observations of the sea surface by coherent L band radar at low grazing angles in a nearshore environment. J. Geophys. Res. 111(C0), 9 015–9 028.

Fu, L.-L., Chelton, D.B., 2001. Large-scale ocean circulation, in: Fu, L.-L., Cazenave, A. (Eds.), Satellite Altimetry and Earth Sciences: A Handbook for Techniques and Applications. Academic Press, San Diego, p. 423, 133–16.

Fu, L.-L., Chelton, D.B., Le Traon, P.-Y., Morrow, R., 2010. Eddy dynamics from satellite altimetry. Oceanography. 23(4), 14–25. http://dx.doi.org/10.5670/oceanog.2010.02.

Fu, L.-L., Ferrari, R., 2008. Observing oceanic submesoscale processes from space. Eos Transactions AGU, 89(48), 488–488. doi: 10.1029/2008EO480003.

Gomez-Enri, J., Cipollini, P., Gommenginger, C., Martin Puig, C., Vignudelli, S., Woodworth, P., Benveniste, J.,Villares, P., 2009. Improving coastal altimeter products by a new retracking approach. Proc. SPIE-Remote Sens. Ocean, Sea Ice, and Large Water Regions, 7473.

Gula, J., Molemaker, M.J., McWilliams, J.C., 2014. Submesoscale cold filaments in the Gulf Stream. J. Phys. Oceanogr. 44, 2617–43.

Grilli, F., Pinardi, N., 1998. The computation of Rossby radii between external forcing mechanisms and internal of deformation for the Mediterranean Sea. MTPNews, 6(4).

Hallberg, R., 2013. Using a resolution function to regulate parameterizations of oceanic mesoscale eddy effects. Ocean Model. 72, 92–103. doi: 10.1016/j.ocemod.2013.08.007.

Heslop, E.E., Sánchez-Román, A., Pascual, A., Rodríguez, D., Reeve, K.A., Faugère, Y., Raynal, M., 2017. Sentinel-3A views ocean variability more accurately at finer resolution. Geophys. Res. Lett. 44, 12367–12374. https://doi.org/10.1002/2017GL076244.

Hu, Z.H., Petrenko, A.A., Doglioli, A.M., Dekeyser, I., 2011. Numerical study of eddy generation in the western part of the Gulf of Lion. J. Geophys. Res. 116, C12030. doi:10.1029/2011JC007074.

Huthnance, M.J., 1995. Circulation, exchange and water masses at the ocean margin: The role of physical processes at the shelf edge. Prog. Oceanogr. 35, 353–431.

Imel, D., 1994. Evaluation of the TOPEX/POSEIDON dual-frequency ionosphere correction. J. Geophys. Res. 99, 24895–24906.

Jebri, F., Zakardjian, B., Birol, F., Bouffard, J., Jullion, L., Sammari, C., 2017. Interannual variations of surface currents and transports in the Sicily Channel derived from coastal altimetry. J. Geophys. Res. Oceans. 122, 8330–8353.

JPL OurOcean Project, 2010. GHRSST Level 4 G1SST Global Foundation Sea Surface Temperature Analysis. Ver. 1. PO.DAAC, CA, USA. http://dx.doi.org/10.5067/GHG1S-4FP01 (accessed 24 May 2017).

Lagerloef, G.S.E., Mitchum, G.T., Lukas, R.B., Niiler, P.P., 1999. Tropical Pacific near-surface currents estimated from altimeter, wind, and drifter data. J. Geophys. Res. 104(C10), 23313–23326.

Lehahn, Y., d'Ovidio, F., Ley, M., Heifetz, E., 2007. Stirring of the Northeast Atlantic spring bloom: A Lagrangian analysis based on multi-satellite data. J. Geophys. Res. Ocean. 112, C08005.

Levy, M., Martin A., 2013. The influence of mesoscale and submesoscale heterogeneity on ocean biogeochemical reactions. Glob. Biogeochem. Cycles. 27, 1139–50.

Mahadevan, A., 2016. The impact of submesoscale physics on primary productivity of plankton. Annu. Rev. Mar. Sci. 8, 161–184.

Marmain, J., Molcard, A., Forget, P., Barth, A., Ourmières, Y., 2014. Assimilation of HF radar surface currents to optimize forcing in the Northwestern Mediterranean Sea. Nonlin. Processes Geophy. 21, 659–675.

Marrec, P., Doglioli, A.M., Grégori, G., Dugenne, M., Della Penna, A., Bhairy, N., Cariou, T., Hélias Nunige, S., Lahbib, S., Rougier, G., Wagener, T., Thyssen, M., 2018. Coupling physics and biogeochemistry thanks to high resolution observations of the phytoplankton community structure in the North-Western Mediterranean Sea. Biogeosciences Discuss. https://doi.org/10.5194/bg-2017-343.

McGillicuddy, D.J., Robinson, A.R., Siegel, D.A., Jannasch, H.W., Johnson, R., Dickey, T.D., McNeil, J., Michaels, A.F., Knap, A.H., 1998. Influence of mesoscale eddies on new production in the Sargasso Sea. Nature. 394, 263–265.

Millot, C., 1999. Circulation in the Western Mediterranean Sea. J. Mar. Syst. 20, 423–442.

Millot, C., 1991. Mesoscale and seasonal variabilities of the circulation in the Western Mediterranean. Dyn. Atm. Oceans, 15, 179–214.

Millot C., TaupierLetage, I., 2005. Circulation in the Mediterranean Sea. The Handbook Environ. Chem. K, 29–66. doi:10.1007/b107143.

Morrow, R., Carret, A., Birol, F., Nino, F., Valladeau, G., Boy, F., Bachelier, C., Zakardjian, B., 2017. Observability of fine-scale ocean dynamics in the Northwestern Mediterranean Sea. Ocean Sci. 13, 13–29. https://doi.org/10.5194/os-13-13-2017.

Muller-Karger, F.E., Varela, R., Thunell, R., Luerssen, R., Hu, C., Walsh, J.J., 2005. The importance of continental margins in the global carbon cycle. Geophys. Res. Lett. 32, L01602. doi:10.1029/2004GL021346.

Nencioli, F., d'Ovidio, F., Doglioli, A.M., Petrenko, A.A., 2013. In situ estimates of submesoscale horizontal eddy diffusivity across an ocean front. J. Geophys. Res. Oceans. 118, 7066–7080. doi:10.1002/2013JC009252.

Palacz, A.P., Pearlman, J., Simmons, S., Hill, K., Miloslavich, P., Telszewski, M., Sloyan, B., Pearlman, F., Bourassa, M., 2017. Report of the workshop on the Implementation of Multi-disciplinary Sustained Ocean Observations (IMSOO). Global Ocean Observing System (GOOS) Report No. 223, http://www.goosocean.org/imsoo-report.

Pascual, A., Bouffard, J., Ruiz, S., Buongiorno Nardelli, B., Vidal-Vijande, E., Escudier, R., 2013. Recent improvements in mesoscale characterization of the

Western Mediterranean Sea: Synergy between satellite altimetry and other observational approaches. Sci. Mar. 77, 19–36. doi: 10.3989/scimar.03740.15a.

Pascual, A., Lana, A., Troupin, C., Ruiz, S., Faugère, Y., Escudier, R., Tintoré, J., 2015. Assessing SARAL data in the coastal zone: Comparisons with HF radar observations. Mar. Geod. 38, sup1, 260–276.

Pascual, A., Ruiz, S., Olita, A., Troupin, C., Claret, M., Casas, B., Mourre, B., Poulain, P-M., Tovar-Sanchez, A., Capet, A., Mason, E., Allen, J.T., Mahadevan, A., Tintoré, J., 2017. A multiplatform experiment to unravel meso- and submesoscale processes in an intense front (AlborEx). Frontiers Mar. Sci. 4, 39. doi: 10.3389/fmars.2017.00039.

Pascual, A., Ruiz, S., Tintore´, J., 2010. Combining new and conventional sensors to study the Balearic current. Sea Technol. 51(7), 32–36.

Passaro, M., Cipollini, P., Vignudelli, S., Graham, D., Quartly, H., Snaith, M., 2014. ALES: A multi-mission adaptive subwaveform retracker for coastal and open ocean altimetry. Remote Sens. Environ. 145, 173–189. ISSN 0034-4257, https://doi.org/10.1016/j.rse.2014.02.008.

Passaro, M., Rose, S.K., Andersen, O.B., Boergens, E., Calafat, F.M., Dettmering, D., Benveniste, J., 2018. ALES+: Adapting a homogenous ocean retracker for satellite altimetry to sea ice leads, coastal and inland waters. Remote Sens. Environ. 211, 456–471. ISSN 0034-4257, https://doi.org/10.1016/j.rse.2018.02.074.

Petrenko, A., 2003. Variability of circulation features in the Gulf of Lions NW Mediterranean Sea: Importance of inertial current. Oceanol. Acta. 26, 323–338.

Pires, N., Fernandes, M.J., Gommenginger, C., Scharroo, R., 2016. A conceptually simple modeling approach for Jason-1 sea state bias correction based on 3 parameters exclusively derived from altimetric information. Remote Sens. 8(7), 576.

Piterbarg, L., Taillandier, V., Griffa, A., 2014. Investigating frontal variability from repeated glider transects in the Ligurian Current (North West Mediterranean Sea). J. Mar. Syst. 129, 381–395. doi: 10.1016/j.jmarsys.2013.08.003.

Poisson, J.C., Quartly, G.D., Kurekin, A., Thibaut, P., Hoang, D., Nencioli, F., 2018. Development of an ENVISAT altimetry processor providing sea level continuity between open ocean and Arctic leads. IEEE Trans. Geosci. Remote Sens. 1–21.

Pond, S., Pickard, G., 2nd Edition 1986. Introductory Dynamical Oceanogrpahy, Pergamon Press Sydney. ISBN 0-08-028728-X

Powell, B.S., Leben, R. R., 2004. An optimal filter for geostrophic mesoscale currents from along-track satellite altimetry. J. Atmos. Oceanic Tech. 21(10), 1633–1642.

Quentin, C., Barbin, Y., Bellomo, L., Forget, P., Gagelli, J., Grosdidier, S., Guerin, C.-A., Guihou, K., Marmain, J., Molcard, A., Zakardjian, B., Guterman, P., Bernardet, K., 2013. HF radar in French Mediterranean Sea: An element of MOOSE Mediterranean Ocean Observing System on Environment, OCOSS'2013 Proceedings, 25–30.

Ralph, E.A., Niiler, P.P., 1999. Wind-driven currents in the tropical Pacific. J. Phys. Oceanogr. 29, 2121–2129.

Ray, R. D., 2013. Precise comparisons of bottom-pressure and altimetric ocean tides, J. Geophys. Res. Oceans. 118, 4570–4584. doi:10.1002/jgrc.20336.

Rio, M.-H., Hernandez, F., 2003. High-frequency response of wind-driven currents measured by drifting buoys and altimetry over the world ocean. J. Geophys. Res. 108(C8), 3283–3301.

Rio, M.-H., Poulain, P.-M., Pascual, A., Mauri, E., Larnicol, G., Santoleri, R., 2007. A mean dynamic topography of the Mediterranean Sea computed from altimetric data, *in situ* measurements and a general circulation model. J. Mar. Sys. 65, 484–508. doi:10.1016/j.jmarsys.2005.02.006.

Rio, M.H., Guinehut, S., Larnicol, G., 2011. New CNES-CLS09 global mean dynamic topography computed from the combination of GRACE data, altimetry, and in situ measurements. J. Geophys. Res. 116, C07018.

Rio, M.-H., 2012. Use of altimeter and wind data to detect the anomalous loss of SVP-type drifter's drogue. J. Atmos. Oceanic Tech. 29, 1663–1674.

Rio, M.-H., Pascual, A., Poulain, P.-M., Menna, M., Barceló, B., Tintoré, J., 2014. Computation of a new mean dynamic topography for the Mediterranean Sea from model outputs, altimeter measurements and oceanographic *in situ* data. Ocean Sci. 10, 731–744. https://doi.org/10.5194/os-10-731-2014.

Ruiz, S., Garau, B., Martnez-Ledesma, M., Casas, B., Pascual, A., Vizoso, G., Bouffard, J., Heslop, E., Alvarez, A. Testor, P., Tintoré, J., 2012. New technologies for marine research: five years of glider activities at IMEDEA. Sci. Mar. 76, p. 261270. 10.3989/scimar.03622.19l http://scientiamarina.revistas.csic.es/index.php/scientiamarina/article/view/1372/1471.

Ruiz, S., Pascual, A., Garau, B., Pujol, I., Tintoré, J., 2009. Vertical motion in the upper ocean from glider and altimetry data. Geophys. Res. Lett. 36:L14607. doi: 10.1029/2009GL038569. L14607.

Shcherbina, A.Y., D'Asaro, E.A., Lee, C.M., Klymak, J.M., Molemaker, M.J., McWilliams, J.C., 2013. Statistics of vertical vorticity, divergence, and strain in a developed submesoscale turbulence field. Geophys. Res. Lett. 40, 4706–11.

Smith, W.H.F., Strub, T., Miller, L., 2008. First coastal altimetry workshop. Eos Trans. AGU. 89(40), 380.

Ssalto/Duacs user handbook, 2016: (M)SLA and (M)ADT near-real-time and delayed-time products, Rep. SALP-MU-P-EA-21065-CLS, Aviso, Ramonville-Saint-Agne, France.

Stanev, E., Beckers, J.-M., Lancelot, C., Le Traon, P., Staneva, J., Peneva, P., Gregoire, M., 2002. Coastal-open ocean exchange. Black Sea examples from survey, satellite data and modelling. Estuar. Coast. Shelf Sci. 54, 601–620.

Strub, T., 2001. High-resolution ocean topography science requirements for coastal studies, in: Chelton, D.B. (Ed.), the Report of the High-resolution Ocean Topography Science Working Group meeting. College of Oceanic and Atmospheric Sciences, Oregon State University, Corvallis, p. 224.

Thomas, L.N., Tandon, A., Mahadevan, A., 2008. Submesoscale processes and dynamics. Ocean Model. Eddying Regime. 17–38.

Tran, N., Vandemark, D., Labroue, S., Feng, H., Chapron, B., Tolman, H.L., Lambin, J., Picot, N., 2010. Sea state bias in altimeter sea level estimates determined by combining wave model and satellite data. J. Geophys. Res. 115, C03020.

Troupin, C., Pascual, A., Valladeau, G., Pujol, I., Lana, A., Heslop, E., Ruiz, S., Torner, M., Picot, N., Tintoré, J., 2015. Illustration of the emerging capabilities of SARAL/AltiKa in the coastal zone using a multi-platform approach. Adv. Space Res. 55(1), 51–59.

Valladeau, G., Thibaut, P., Picard, B., Poisson, J.C., Tran, N., Picot, N., Guillot, A., 2015. Using SARAL/AltiKa to improve Ka-band altimeter measurements for coastal zones, hydrology and ice: The PEACHI prototype. Mar. Geod. 38(S1), 124–142. doi: 10.1080/01490419.2015.1020176.

Verron, J., Sengenes, P., Lambin, J., Noubel, J., Steunou, N., Guillot, A., Picot, N., Coutin-Faye, S., Sharma, R., Gairola, R.M., Murthy, R.D.V.A., Richman, J.G., Griffin, D., Pascual, A., Rémy, F., Gupta, P.K., 2015. The SARAL/AltiKa altimetry satellite mission, Mar. Geod. 38, sup1, 2–21. doi: 10.1080/01490419.2014.1000471.

Vignudelli, S., Cipollini, P., Roblou, L., Lyard, F., Gasparini, G.P., Manzella, G., Astraldi, M., 2005. Improved satellite altimetry in coastal systems: Case study of the Corsica Channel (Mediterranean Sea). Geophys. Res. Lett. 32, L07608. doi:10.1029/2005GL022602.

Vignudelli, S., Kostianoy, A., Cipollini, P., Benveniste, J., 2011. Coastal , DOIaltimetry. doi: 10.1007/978-3-642-12796-0.

Zakardjan, B., Prieur L., 1998. Biological and chemical signs of upward motions in permanent geostrophic fronts of the Western Mediterranean. J. Geophys. Res. 103, 27849–27866.

List of Figure Captions

Figure 11 OSCAHR cruise transects (in letters) showing MVP vertical salinity profiles (coloured rectangles), geo-located with altimetric tracks #9 from Jason-2 and tracks #429 and #674 from SARAL. The main flow of the NC is shown with black arrows, the recirculation with the grey arrow and the Ligurian Sea area is highlighted by the red box.

Figure 12 PEACHI high rate altimetry SLA editing and filtering for SARAL track #429. The black line corresponds to the AVISO 1 Hz track.

Figure 13 RIO07 (a) and RIO14 (b) MDT overlapped by the derived mean current.

Figure 14 Reference depth sensitivity study for transects A – B, D – A, G – I and H – G. Different colours are associated with a different reference depths (in meters) considered in the vertical integration of MVP data, while PEACHI altimetry data are shown in black. The magenta line represents the MVP derived currents at the maximum operating depth. The shaded grey areas in transects A – B and D – A correspond to 20 km from the coast.

Figure 5 Mean (blue) and standard deviation (yellow) of the current differences between PEACHI and MVP.

Figure 6 Geographical plot of the differences (coloured dots) of the surface across track current ADCP-MVP. The vectors are related to the cross-track component of the ADCP current at 270 m depth.

Figure 7 Comparison between MVP (magenta) and ADCP currents (raw data in thin blue, filtered and smoothed data in dashed thick blue) for each transect.

Figure 15 PEACHI Altimetry (grey for SLA+RIO07 and red for adaptive retracking, cyan for Red3 retracking and green for MLE4 retracking for SLA+RIO14) vs AVISO altimetry (light grey for SLA+RIO07 and grey for SLA+RIO14) vs *in situ* (magenta for MVP, blue for ADCP). Different markers for both AVISO and PEACHI altimetry are related to elevations and currents computed with a different MDT (crosses for RIO07 and diamonds for RIO14). First column reports track geolocation, second column reports ADT (m) vs Latitude and third column reports satellite across track current (ms-1) derived from ADT computed adding RIO14 to SLA vs Latitude together with in situ derived current vs Latitude. The distance to the coast is also reported in Kilometres.

Figure 16 Surface circulation pattern derived from *in situ* (magenta for MVP and blue for ADCP) and PEACHI altimetry data (black). SST data is also shown with a Spatial Resolution of 0.062º (Latitude) x 0.062º (Longitude) and temporal resolution of 1 day. The SST maps is an average over the OSCAHR cruise time period (29th October 2015 to 6th November 2015). White arrows depict the surface oceanographic features reported also in Figure 10 vertical profiles.

Figure 17 MVP Salinity and temperature vertical profiles. The oceanographic features are reported with white arrows.